Chronological control and centennial-scale climatic subdivisions of the Last Glacial Termination in the western Mediterranean region

Camuera, Jon

2021-03-01

Camuera , J , Jimenez-Moreno , G , Ramos-Roman , M J , Garcia-Alix , A , Jimenez-Espejo , F J , Toney , J L & Anderson , R S 2021 , ' Chronological control and centennial-scale climatic subdivisions of the Last Glacial Termination in the western Mediterranean region ' , Quaternary Science Reviews , vol. 255 , 106814 . https://doi.org/10.1016/j.quascirev.2021.106814

http://hdl.handle.net/10138/333551
https://doi.org/10.1016/j.quascirev.2021.106814

Quaternary Science Reviews 255 (2021) 106814

Contents lists available at ScienceDirect

Quaternary Science Reviews

journal homepage: www.elsevier.com/locate/quascirev

Chronological control and centennial-scale climatic subdivisions of the Last Glacial Termination in the western Mediterranean region

Jon Camuera [a, *], Gonzalo Jiménez-Moreno [b], María J. Ramos-Román [a], Antonio García-Alix [b, c], Francisco J. Jiménez-Espejo [c], Jaime L. Toney [d], R. Scott Anderson [e]

[a] Department of Geosciences and Geography, Faculty of Science, University of Helsinki, Finland
[b] Departamento de Estratigrafía y Paleontología, Universidad de Granada, Spain
[c] Instituto Andaluz de Ciencias de la Tierra (IACT), Consejo Superior de Investigaciones Científicas-Universidad de Granada (CSIC-UGR), Spain
[d] School of Geographical and Earth Sciences, University of Glasgow, UK
[e] School of Earth and Sustainability, Northern Arizona University, USA

ARTICLE INFO

Article history:
Received 1 October 2020
Received in revised form
23 December 2020
Accepted 13 January 2021
Available online 3 February 2021

Handling Editor: Donatella Magri

Keywords:
Paleoclimate
Iberian peninsula
Pollen analysis
Last glacial
Heinrich stadial 1
Solar activity

ABSTRACT

The Last Glacial Termination is marked by changing environmental conditions affected by abrupt and rapid climate oscillations, such as Heinrich Stadial 1 (HS1), which is characterized by extremely low sea surface temperatures (SST) and significant changes in northern hemisphere terrestrial landscape (e.g., vegetation) and human dispersion. Previous studies show that overall cold/dry conditions occurred during HS1, but the lack of high-resolution records precludes whether climate was stable or instead characterized by instability. A high-resolution paleoclimatic record from the Padul wetland (southern Iberian Peninsula), supported by a high-resolution chronology and contrasted with other records from southern Europe and the Mediterranean region, shows 1) that the age boundaries of HS1 in this area occurred at ~18.0 kyr BP (median age = 17,970 cal yr BP; mean age = 18,030 ± 330 cal yr BP) and ~15.2 kyr BP (median age = 15,210 cal yr BP; mean age = 15,200 ± 420 cal yr BP) and 2) that climate during HS1 was non-stationary and centennial-scale variability in moisture is superimposed on this overall cold climatic period. In this study, we improve the pollen sampling resolution with respect to previous studies on the same Padul-15-05 sedimentary core and suggest a novel subdivision of HS1 in 7 sub-phases, including: i) 3 sub-phases (a.1-a.3) during an arid early phase (HS1a; ~18.4–17.2 kyr BP), ii) a relatively humid middle phase (HS1b; ~17.2–16.9 kyr BP), and iii) 3 sub-phases (c.1-c.3) during an arid late phase (HS1c; ~16.9–15.7 kyr BP). This climatic subdivision is regionally supported by SST oscillations from the Mediterranean Sea, suggesting a strong land-sea coupling. A cyclostratigraphic analysis of pollen data between 20 and 11 kyr BP indicates that the climate variability and the proposed subdivisions characterized by ~2000 and ~800-yr periodicities could be related to solar forcing controlling climate in this area.

1. Introduction

The Last Glacial Termination in southern Europe and Mediterranean areas present one the most inhospitable environmental conditions of the last 130 kyr, reaching one of the lowest SST record for this period (Martrat et al., 2004, 2007). During the last deglaciation, HS1 shows abrupt and complex climate signals under the roughest conditions, as observed by the presence of ice-rafted debris during Heinrich events (Hodell et al., 2017), the slowdown of Atlantic and Mediterranean thermohaline circulations (McManus et al., 2004; Sierro et al., 2020) and major genetic bottlenecks in humans (Fernández-López de Pablo et al., 2019). In this respect, deciphering rapid (e.g., millennial-scale) climate changes and environmental impacts due to Dansgaard/Oeschger and Heinrich-like climatic oscillations during the last glacial period and deglaciation have been the aim of ice, marine and terrestrial paleoclimate investigations (Cacho et al., 2006; Höbig et al., 2012; Panagiotopoulos et al., 2014; Sánchez Goñi et al., 2008).

The different Heinrich nomenclatures, that is Heinrich Events (HEs), Heinrich Layers (HLs) and Heinrich Stadials (HSs), has caused

* Corresponding author.
E-mail addresses: jon.camuera@helsinki.fi, jcamuera@gmail.com (J. Camuera).

https://doi.org/10.1016/j.quascirev.2021.106814

much confusion in the scientific literature. HEs refer to massive discharge of ice-rafted debris (IRD) from Laurentide, Fenno-scandian and Greenland ice sheets into the North Atlantic, resulting in the deposition of detrital and carbonate-rich sediment layers called HLs (Heinrich, 1988; Hemming, 2004; Hodell et al., 2017). HSs were described as cold temperature intervals revealed in the North Atlantic records during which HEs occurred (Barker et al., 2009). These periods and events represent the most extreme glacial conditions, which resulted from the culmination of the decreasing temperature trends of Bond cycles (Bond et al., 1993).

Several marine paleoclimatic records evidenced the effect of especially cold and arid conditions recorded during HSs, also with strong direct influence in terrestrial records (Fletcher and Sánchez Goñi, 2008; Fletcher et al., 2010a; Hodell et al., 2017; Martrat et al., 2014; Moreno et al., 2010). HS1 is the most recent and one of the coldest Heinrich Stadials of the last glacial cycle and has been described in several marine sedimentary records nearby the study area (Naughton et al., 2016; Salgueiro et al., 2014).

However, different records show chronological discrepancies in the onset and the end of this period (Fletcher et al., 2010b; Moreno et al., 2010; Sánchez Goñi and Harrison, 2010). Causes in age differences in the environmental responses obtained from different records in the same region to HS1 can be a consequence of: a) errors/uncertainties from dating techniques, b) poor age control produced by low sample resolution, c) very low sedimentary rates, precluding an accurate chronological control, d) the reservoir effect in marine sediments deposited during HS1 in the North Atlantic [~500–1300 ^{14}C years according to Stern and Lisiecki (2013)] and Mediterranean Sea [~800 years according to Siani et al. (2001)] and/or, e) the reworked materials in both marine and continental areas.

High-resolution paleoclimatic records show that climate during HS1 was characterized by short-scale internal variability (Dupont et al., 2010; Escobar et al., 2012; Stager et al., 2011; Stríkis et al., 2015; Zhang et al., 2014). However, few studies have focused on short-term internal climate variability of HSs in southern Europe and the western Mediterranean region, and in particular within HS1 (Fletcher and Sánchez Goñi, 2008). In this regard, a division of HS1 into two and three phases has previously been observed in very few marine records. For example, two phases were described in Iberian margin marine sedimentary records (Naughton et al., 2009; Salgueiro et al., 2014; Sánchez Goñi et al., 2018) and Nile River Basin (Castañeda et al., 2016), characterized by similar wet conditions during the first phase and arid climate during a second phase. Other paleoclimate studies recorded a three-phase division for HS1, including studies from the Alboran Sea (Bazzicalupo et al., 2018; Fletcher and Sánchez Goñi, 2008), northwestern Mediterranean (Sierro et al., 2005), Iberian margin (Naughton et al., 2016; Sierro et al., 2020; Voelker et al., 2009) and off NW Africa (Bouimetarhan et al., 2012) (Table 1). Nevertheless, the studies showing a three-phase division of HS1 disagree in the paleoenvironmental characterization of each phase and a complete knowledge of the variability within HS1 has yet to be achieved (Hodell et al., 2017).

This study aims to improve the resolution of the pollen analysis for the HS1 time-period from a previous palynological study covering the last two glacial-interglacial cycles in the Padul-15-05 terrestrial sedimentary record (southern Iberian Peninsula) (Camuera et al., 2019). As a result, we present high-resolution pollen and sedimentological data between 20 and 11 kyr BP, registering regional vegetation and local lake paleoenvironmental responses to climate changes during the last glacial-Holocene transition, including HS1, Bølling-Allerød (BA) and Younger Dryas (YD). In order to have a good chronological control of HS1 in southern Europe and the Mediterranean region, we have compiled, revised, recalibrated and modelled the HS1 age-boundaries from non-tuned and independently dated high-resolution marine and terrestrial paleoclimatic records from this region.

2. Regional and local settings

The Padul wetland (724 m a.s.l.) is located in the western margin of the Sierra Nevada range, 20 km south of Granada city (Andalusia, Spain) and covers an area of 4 km^2 in the Padul-Nigüelas basin (Fig. 1). The NW-SE elongated Padul-Nigüelas endorheic basin developed as a consequence of extensional activity of the main normal fault that delimits the NE edge of the basin (Santanach et al., 1980). The catchment of the basin comprises mainly Triassic limestone/dolomite and Cambrian-Triassic schists, whereas the basin fill sediments are principally Miocene gypsum and detritics, and Quaternary peat and alluvial deposits (Camuera et al., 2018). It bears an estimated sedimentary sequence of about 100 m in the depocenter of the basin (Ortiz et al., 2004).

The precipitation in the region is highly controlled by the humidity carried from the westerlies and the North Atlantic Oscillation (Jiménez-Moreno and Anderson, 2012; Lionello, 2012). At present, the Padul area is characterized by a semiarid Mediterranean climate with high temperature and low precipitation during summertime (summer drought), presenting a mean annual temperature of 14.4 °C and mean annual precipitation of 445 mm (AEMET, 2016).

The present-day vegetation in the Padul wetland is mainly characterized by wetland communities, such as *Phragmites australis* and *Typha domingensis*, whereas the surrounding areas are dominated by mesomediterranean vegetation with *Quercus rotundifolia*, *Q. faginea*, *Q. coccifera*, *Pistacia terebinthus*, *Populus alba*, *Ulmus minor*, *Fraxinus angustifolia* and *Celtis australis*, among others.

3. Materials and methods

3.1. Padul chronology

The 42.64 m-long Padul-15-05 sediment core was drilled in the Padul wetland lakeshore (37°00′39"N, 3°36′14"W) in July 2015 (Fig. 1). The chronological control of the entire Padul-15-05 core was based on 43 Accelerator Mass Spectrometry (AMS) radiocarbon dates, 4 Amino Acid Racemization (AAR) dates from gastropods (*hydrobiid Milesiana schuelei*) and two different sediment accumulation rates (SAR) for both peat and carbonate/marl lithologies for the bottom part of the core, showing the record of the last ~200 kyr (Camuera et al., 2018). In addition, six new AMS radiocarbon samples (from ~15.6 to ~19.4 kyr BP) have been analyzed in this study to better delimit the age range of HS1 (Table S1).

In this study a new Bayesian age-depth model has been built for the last 30 kyr BP. This new age model, developed using the R-based BACON software (v.2.3.9.1 - July 2019) (Blaauw and Christen, 2011), is based on 40 radiocarbon dates (including specific compound radiocarbon dating), providing a more detailed and accurate chronological control and taking into account age uncertainties (Fig. 2 and Tables S1 and S2). The age model suggests a good fitting (stable output of the log-posterior time-series) and a robust Markov Chain Monte Carlo mixing (Gelman and Rubin Reduction Factor (1.016) under the safety threshold of 1.05 (Brooks and Gelman, 1998)). The parameters of the model are included in Fig. 2. The high-resolution age-depth model shows high sediment accumulation rates (SAR, 0.155 mm/yr) during this time period, and therefore, allows for the development of regional paleoclimate reconstructions from high-resolution multiproxy analyses. Note that all the ages from the Padul record provided throughout the manuscript are calibrated kiloyears before present expressed as kyr BP to simplify.

Table 1
Marine records presenting a division of HS1 in three phases (Bazzicalupo et al., 2018; Bouimetarhan et al., 2012; Fletcher and Sánchez Goñi, 2008; Naughton et al., 2016; Sierro et al., 2005, Sierro et al., 2020; Voelker et al., 2009). Marine and continental reconstructions of the early, middle and late HS1 have been schematized. Note the diversity in the interpretations for the three phases identified within HS1.

Study	Location	Record	Environment	Proxy	Early HS1 (HS1a)	Middle HS1 (HS1b)	Late HS1 (HS1c)
Fletcher and Sánchez Goñi (2008)	Alboran Sea	MD95-2043	Marine	*N. pachyderma-s* (cold water indicator)	Cool	Cold	Cool
			Continental	Vegetation	Cold/humid	Arid	Cool/less arid
Bazzicalupo et al. (2018)	Alboran Sea	ODP-976	Marine	Calcareous plankton	Cold	Fresher water	Cooler
			Continental	Vegetation	Increase aridity	Maximum aridity	Cold/arid
Sierro et al. (2005)	Northwestern Mediterranean	MD99-2343	Marine	δ^{18}O *G. bulloides* (SST, iceberg meltwater)	Cold	Cool	Cold
Naughton et al. (2016)	Iberian margin	MD03-2697	Marine	Alkenone-based SST and % *N. pachyderma-s*	Extreme cooling	Warmer (still cool)	Cooling (warmer than HS1a)
			Continental	Vegetation	Extreme cold/wet	Warmer (still cool)/ increase aridity	Warming/wet
Voelker et al. (2009), Sierro et al. (2020)	Iberian margin	MD99-2339	Marine	SST and δ^{18}O seawater	Cold	Warmer	Cold
Bouimetarhan et al. (2012)	Off NW Africa	GeoB9508-5	Continental	Vegetation	Dryness	Wetter	Extreme dry

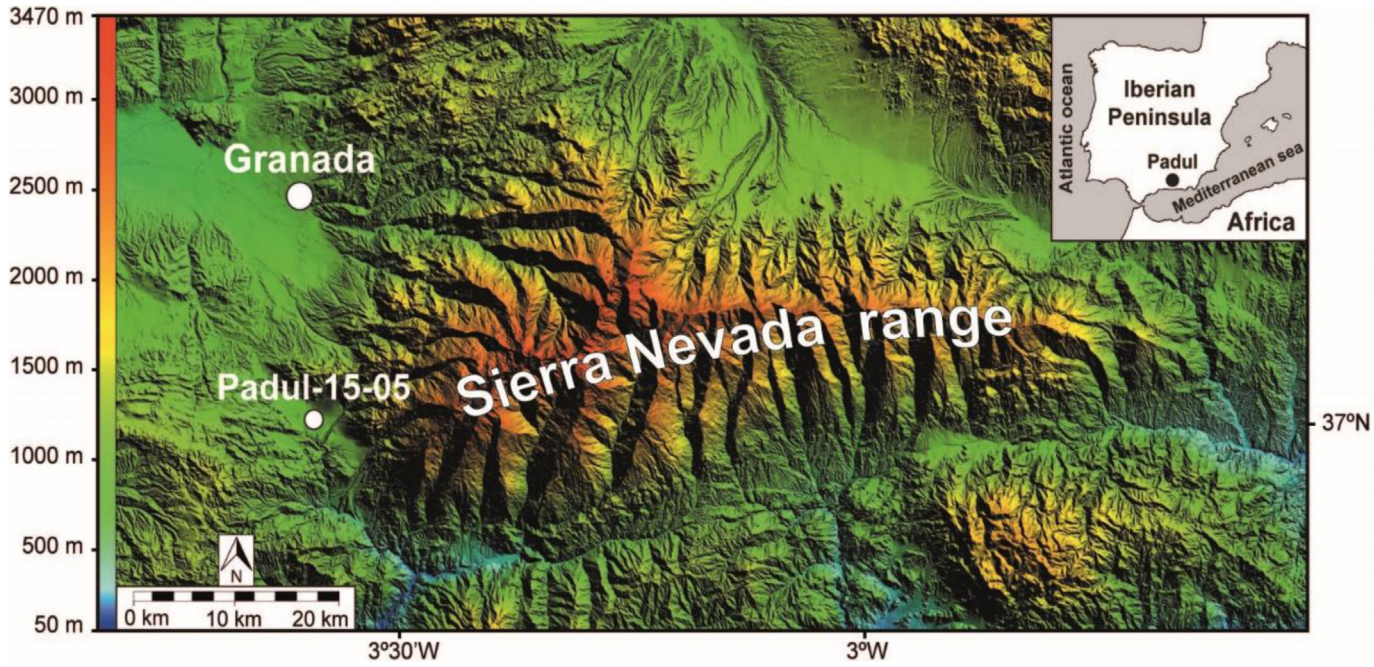

Fig. 1. Geographical location of the Padul-15-05 record in the western margin of Sierra Nevada range and south of Granada city (southern Iberian Peninsula) (modified from Camuera et al., 2018).

3.2. Chronological analysis of HS1 in southern Europe and the Mediterranean region

In order to compare and corroborate the good time delimitation of HS1 in Padul, the age-range (onset and end) for HS1 in southern Europe and the Mediterranean region was statistically calculated using a compilation of available marine and terrestrial (lakes, speleothems) sites recording HS1 in this area.

The compilation of these records was done according to the following criteria:

1) Records are located in southern Europe and the Mediterranean region, specifically, between latitude 31°N and 48°N, and between longitude 10°W and 34°E.
2) Records are of high-resolution data only, where HS1 is represented with at least 10 samples (ca. <250-yr mean resolution).
3) In order to avoid circular reasoning, records should not be tuned to ice-core chronologies or to other nearby records, and ages for HS1 should be based on independent absolute dates providing an objective age-depth model.
4) Records should have an exact numerical age-range for HS1 suggested or mentioned in the corresponding original studies.

High-resolution marine and terrestrial paleoclimatic records from 17 sites (including Padul-15-05) with non-tuned and independent chronology have been compiled following the above criteria (Figs. S1 and S2). We selected the most sensitive paleoclimatic proxies responding to HS1 from each study site and those chosen by authors as the most representative indicators of

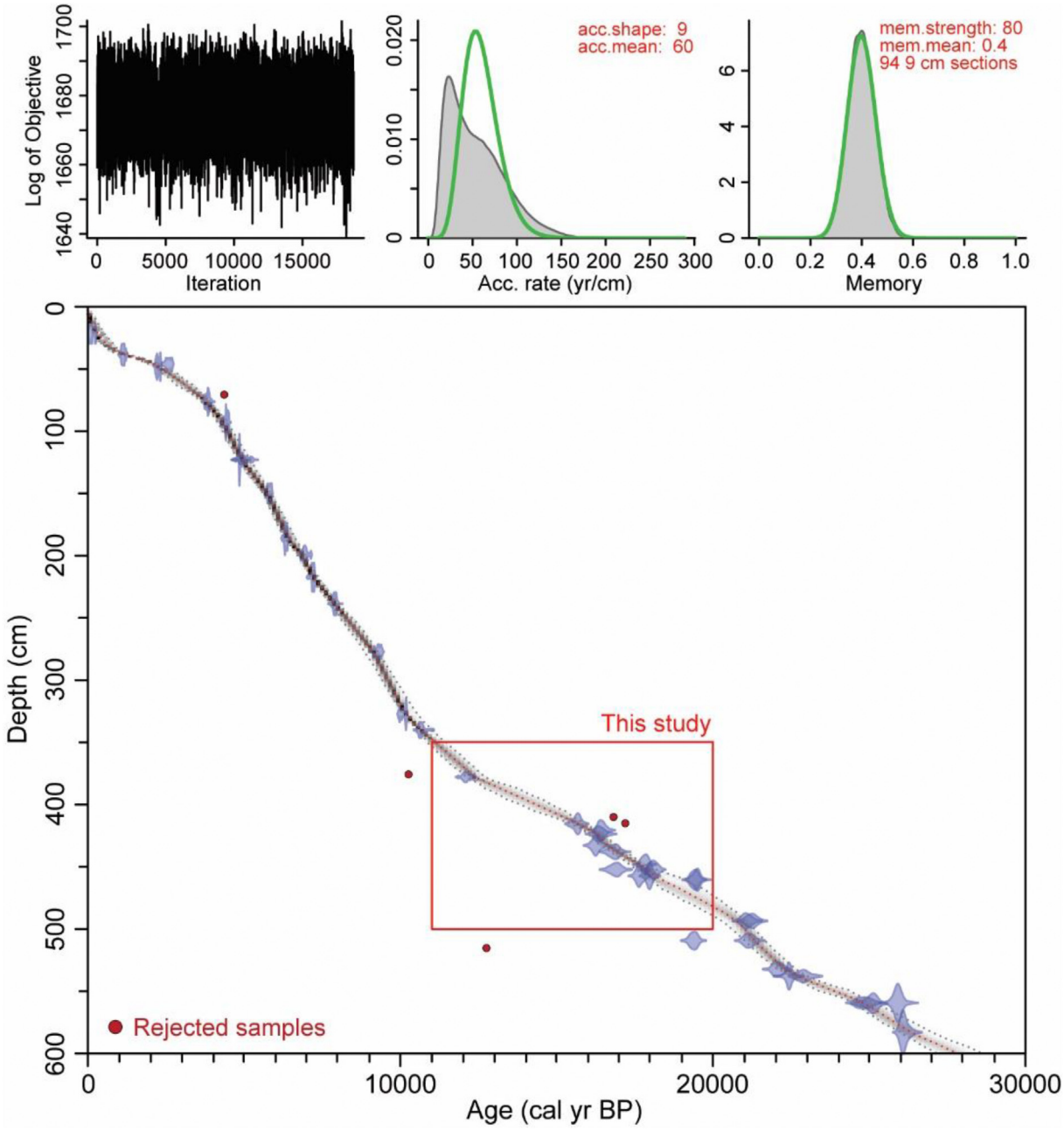

Fig. 2. Bayesian age-depth model of the Padul-15-05 record for the last 30 kyr BP. The red square shows the discussed period in this study (20–11 kyr BP). See Tables S1 and S2 for specific information about the radiocarbon samples. Acronyms: acc. shape, accumulation shape; acc. mean, accumulation mean, mem. strength, memory strength; mem. mean, memory mean. (For interpretation of the references to color in this figure legend, the reader is referred to the Web version of this article.)

environmental changes. Even if the compiled paleoclimatic proxies represent different environmental signals (aridity, freshwater pulses, presence of cold water, etc.), the lack of enough records displaying the same signal as in Padul (aridity, temperature) under the criteria mentioned above does not allow us to suggest an age-range for HS1 based on a unique climate signal.

The revision of HS1 age boundaries of the compiled records was done by 1) choosing the middle-points of HS1 climate transitions (i.e., Last Glacial Maximum-HS1 transition for the onset of HS1 and HS1-Bølling Allerød transition for the end of HS1), according to previous studies (e.g., Fletcher et al., 2010a, b; Rasmussen et al., 2014), and 2) taking the points presenting significant environmental changes closer to the HS1 boundaries provided by authors in each study (Fig. S2 and Table S3). Uncalibrated ages (^{14}C age ± error) of the revised HS1 age boundaries from each record were calculated by the means of the original ^{14}C calibration curves used in each study. Afterwards, the uncalibrated ages were independently recalibrated using recent calibration curves (IntCal13, Marine13) (Fig. 3 and Table S3). With respect to the U/Th ages from the CAN speleothem (Pindal cave), we have taken the ages boundaries from the U/Th-based age model (^{230}Th corrected age) of the original study (Moreno et al., 2010). The modelled age-ranges of HS1 for each record were calculated running a Kernel Density Estimation_*plot* (*KDE_plot*) function with a Bayesian approach using the Oxcal software (Ramsey, 2017). This methodology was also applied combining all these records (*KDE Total*) to obtain a

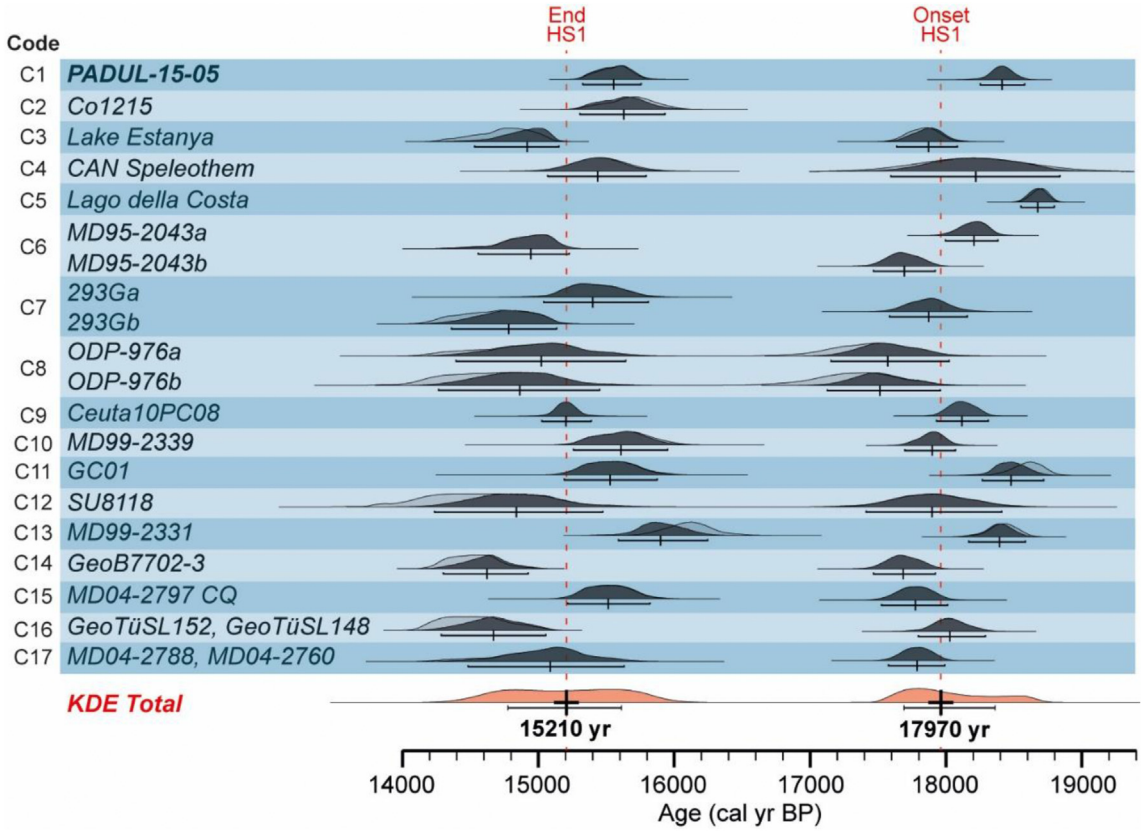

Fig. 3. Median ages of HS1 boundaries, obtained by means of a *KDE_plot* function under a Bayesian modelling. The probability distribution of the Gaussian (light shades) and Bayesian-modelled ages (dark shades) are shown with the 2σ standard deviations and the median values (horizontal and small vertical lines below probability distributions). For the *KDE Total*, the horizontal lines below the distributions show the 1σ standard deviation. Ages for each non-tuned high-resolution records have been obtained according to our revision of the age boundaries from the paleoclimatic data to HS1 (green dots in Figure S2) and recalibrated to recent age calibrations (IntCal13, Marine13). Red vertical dashed lines indicate the median age distributions of the HS1 boundaries provided by the *KDE Total* (onset HS1 = 17,970 cal yr BP; end HS1 = 15,210 cal yr BP). Codes (C1, C2, C3 …) have been used for an easier identification of records. (For interpretation of the references to color in this figure legend, the reader is referred to the Web version of this article.)

synthetic regional model for the age-range of HS1 (Fig. 3).

3.3. Palynological analysis

In this study, the resolution of the pollen data has been increased with 24 new pollen samples with respect to the previous study from the Padul-15-05 record by Camuera et al. (2019), resulting in a total of 91 pollen samples between 4.82 and 3.47 m depth (20–11 kyr BP). Therefore, the new sample resolution for HS1 (18.4–15.7 kyr BP) is ~61 years, and ~127 years for the Bølling-Allerød (BA), Younger Dryas (YD) and the beginning of the Holocene (15.7–11 kyr BP).

The pollen extraction was done following a modified methodology of Faegri and Iversen (1989). After the final extraction of the pollen residue, a minimum of 300 terrestrial pollen grains per sample were identified using a transmitted light microscope. Percentages of all pollen taxa were calculated based on the terrestrial pollen sum excluding aquatic plants (Cyperaceae, *Typha*, *Myriophyllum*, *Utricularia* and *Potamogeton*). The detailed pollen diagram has been represented in Figure S3 using the Tilia software (Grimm, 1987). The zonation of the pollen data was done on the main pollen taxa (i.e., *Quercus* total, *Olea*, *Pistacia*, Cupressaceae, *Artemisia* and Amaranthaceae) using the constrained cluster analysis (CONISS) in order to identify pollen zones and the climatic subdivision of the HS1, BA and YD periods (Fig. S3). *Pinus* total was excluded from the cluster analysis because it is overrepresented during some periods, as in other Iberian studies (García-Antón et al., 2011; Morales-Molino et al., 2011).

The Mediterranean forest, xerophytes, Pollen Climate Index (PCI) and Precipitation Index (I_p) have been used as pollen paleoclimatic proxies (Fig. 4c–f and Fig. 5a). The Mediterranean forest (sum of *Quercus* total, *Olea*, *Phillyrea* and *Pistacia*) and xerophytes (sum of *Artemisia*, *Ephedra* and Amaranthaceae) have previously been shown to be a good indicator of climate changes in the Mediterranean region (Fletcher and Sánchez Goñi, 2008; Ramos-Román et al., 2018a). The PCI is based on the ratio of mesothermic taxa (sum of *Quercus* total, *Olea*, *Fraxinus*, *Phillyrea*, *Acer*, *Betula*, *Alnus*, *Ulmus*, *Taxus*, *Salix*, *Pistacia, Corylus* and *Carpinus*) divided by steppic taxa (sum of *Artemisia*, *Ephedra*, *Hippophaë* and Amaranthaceae) (Combourieu Nebout et al., 1999; Joannin et al., 2011), and has been useful in identifying climate changes mainly related to temperature in this region (Bertini et al., 2015; Camuera et al., 2019). However, some taxa included in the PCI also respond to different precipitation conditions, hence a more precise reconstruction of the precipitation in this area has been obtained using the *Ip* (Fletcher et al., 2010b). The *Ip* is expressed as: *Ip* = *Quercus* deciduous/(*Artemisia* + *Ephedra* + Amaranthaceae + *Quercus* deciduous).

3.4. Inorganic geochemistry

The inorganic elemental geochemistry data of the last ~200 kyr of the Padul-15-05 record show paleoenvironmental changes related to orbital- and suborbital-scale climate fluctuations

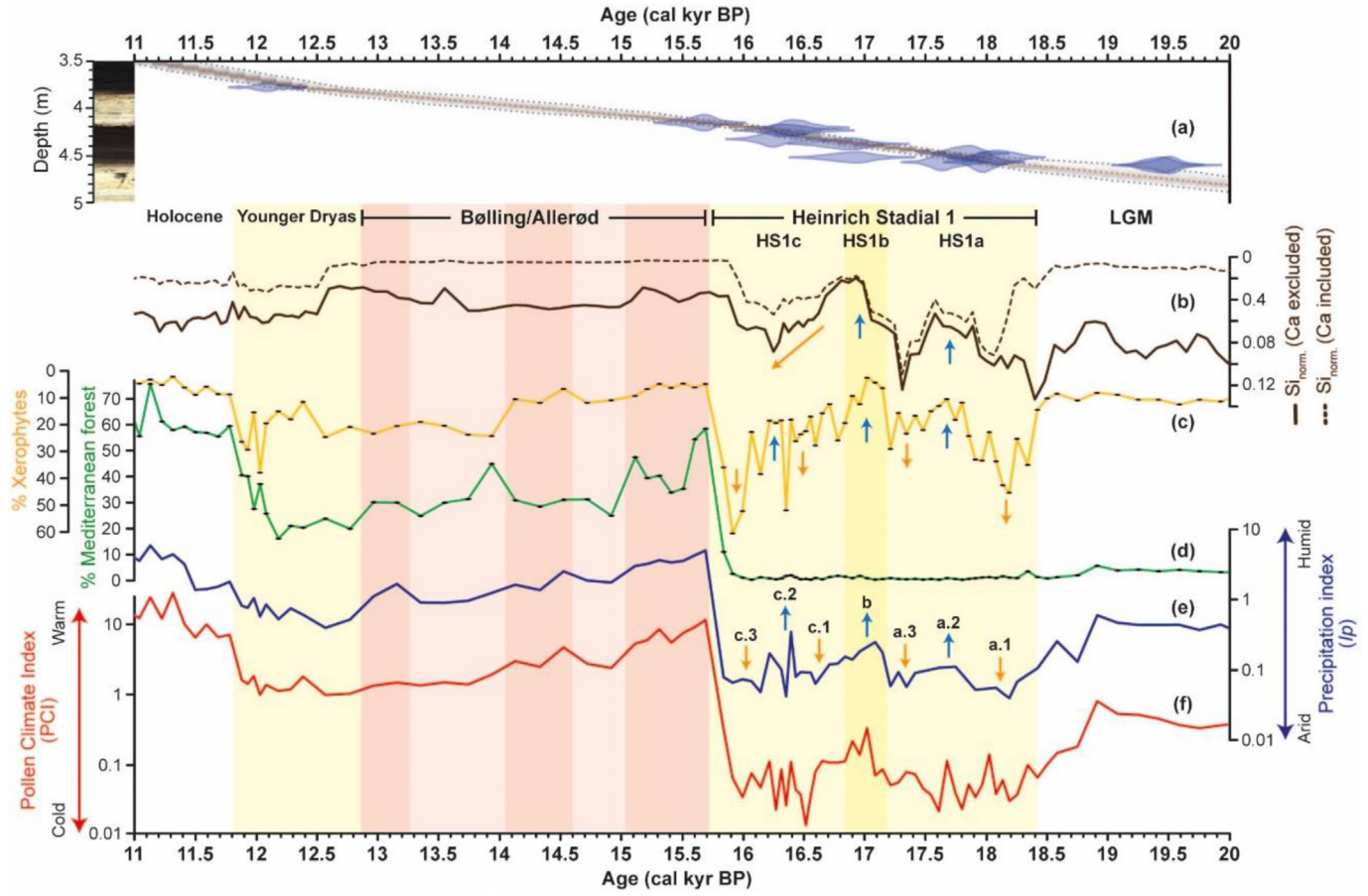

Fig. 4. Paleoclimatic raw data from the Padul-15-05 sediment core for the time period between 20 and 11 kyr BP: (a) Core photograph and age-depth model for the studied period. (b) Normalized silicon values, with calcium excluded (continuous line) and included (dashed line) from total counts (values inverted). (c) Percentage of xerophytes (values inverted). (d) Percentage of Mediterranean forest. (e) Precipitation Index (*Ip*). (f) Pollen Climate Index (PCI). Yellow shadings show the Younger Dryas (YD) and Heinrich Stadial 1 (HS1). Dark yellow shading within HS1 indicates the slightly warmer/wetter middle phase (HS1b). Blue arrows indicate the moderately warmer/wetter sub-phases within HS1, whereas orange arrows show the colder/more arid sub-phases. Dark and light red shadings show the Bølling-Allerød (BA): dark red shadings correspond to the warmer/wetter periods (similar to Greenland Interstadials 1e, 1c and 1a; Rasmussen et al., 2014), whereas light red shadings correspond to the colder/more arid events (similar to Greenland Interstadials 1 d and 1 b; Rasmussen et al., 2014). See Figure S3 for the detailed pollen diagram of the main pollen taxa. The complete pollen dataset can be found in the PANGAEA data repository (https://doi.pangaea.de/10.1594/PANGAEA.904053). (For interpretation of the references to color in this figure legend, the reader is referred to the Web version of this article.)

(Camuera et al., 2018). Silicon was used as indicator of siliciclastic input from the Sierra Nevada into the wetland and was taken as the most representative inorganic element for environmental reconstructions (Camuera et al., 2018). In this study, we present Si data with a sampling resolution of ~67 years for the time period between 20 and 11 kyr BP. This element has been used as Si normalized (Si_{norm}), represented by the silicon data divided by the sum of the total counts (in cps) from the most important elements (Si, K, Ca, Fe, Zr, Br, Sr, Al, Rb, Cl, Zn, Mn, S, Pb, U, Ni and Ti). As calcium presents very high values in carbonate lithologies, normalized Si values excluding Ca from the total counts is also shown in order to better observe changes in Si content in carbonate-rich sediments (Fig. 4b).

3.5. Test of statistical significance (SiZer)

In order to observe the internal environmental oscillations occurring during HS1 and the significance level of these changes, the "Significant Zero crossing of derivatives" (SiZer) method was run on the 3-point moving average xerophyte percentages from Padul between 19 and 15 kyr BP. The SiZer method examines the derivatives of a curve for identifying the presence of a threshold and finds where the derivative of a function of an environmental variable changes significantly (Chaudhuri and Marron, 1999). This approach was done using the "SiZer" package from the R software (www.cran.r-project.org), using the locally weighted polynomial regression technique (Fan and Gijbels, 1996) for estimating the two derivatives and threshold. This analysis has also been used for identifying the significance of the environmental and climate changes from several past and present (paleo)environmental data (Giesche et al., 2019; Hald et al., 2004; Sonderegger et al., 2009).

The first derivative in the SiZer analysis shows the general trends of statistically significant increasing (red color) or decreasing (blue color) functions, whereas the second derivative gives information about the curvature of the data, pointing into concave up (blue color) or concave down (red color) features. The SiZer map is represented in purple when the derivatives have values 0 (or close to 0) and cannot be concluded to have either decreasing or increasing functions (nor trends), whereas the gray areas indicate regions where the data are too sparse to make statements about significance (Chaudhuri and Marron, 1999) (Fig. 6).

3.6. Spectral analysis

A cyclostratigraphic spectral analysis was performed on xerophyte percentages for the age range between 20 and 11 kyr BP from

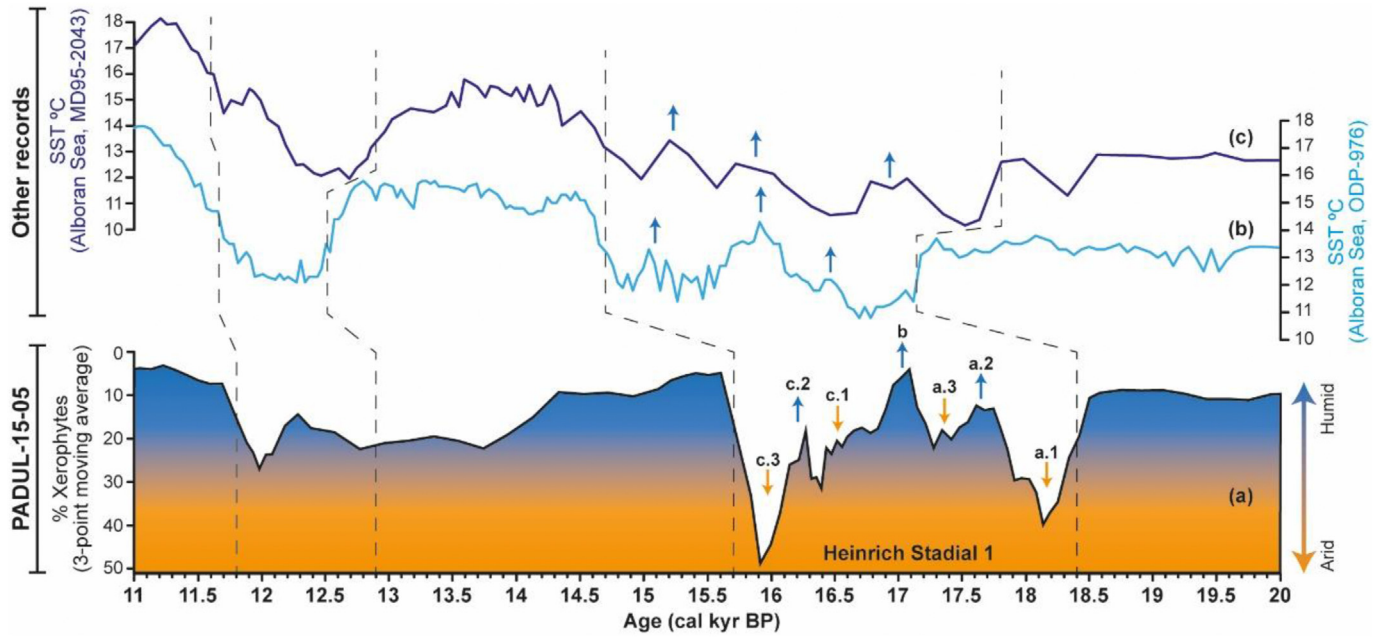

Fig. 5. Paleoclimatic data from Padul and Alboran Sea for the time period between 20 and 11 kyr BP: (a) Xerophyte data from Padul-15-05 with three-point moving average (values inverted). (b) SST (°C) from ODP-976 record of Alboran Sea (Martrat et al., 2014). (c) SST (°C) from MD95-2043 record of Alboran Sea (Cacho et al., 1999, 2006). Within HS1, blue and orange arrows in the Padul record show the relatively humid and arid sub-phases, respectively. In the SSTs from Alboran Sea during HS1, blue arrows marked the warmer temperatures in relation with the relatively more humid sub-phases from Padul (HS1a.2, HS1b and HS1c.2). Vertical dashed lines (from right to left) show transitions between Last Glacial Maximum-HS1, HS1-BA, BA-YD and YD-Holocene for each study. (For interpretation of the references to color in this figure legend, the reader is referred to the Web version of this article.)

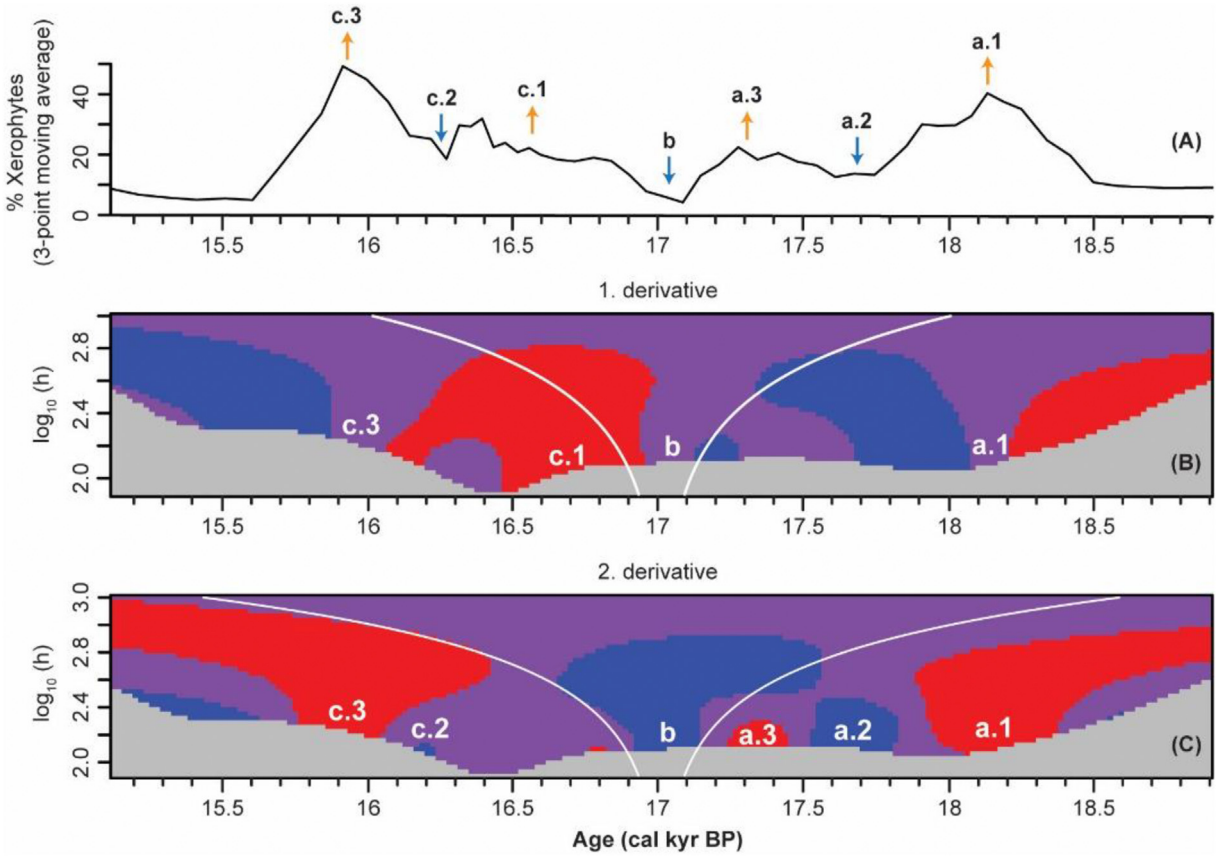

Fig. 6. Test of statistical significance based on the SiZer method and run on (A) the 3-point moving average xerophyte percentages from Padul between 19 and 15 kyr BP. The *y* axis in the first derivative (figure B) and second derivative (figure C) show the bandwidth parameter *h* in units log(*h*). Blue and orange arrows show (as in previous figures) the relatively humid and arid sub-phases, respectively. (For interpretation of the references to color in this figure legend, the reader is referred to the Web version of this article.)

the Padul-15-05 record with the purpose of identifying cyclicities related to regional climate oscillations (Fig. 7). Xerophytes abundance has been proven to be a good proxy for regional moisture availability in this area (Pini et al., 2009; Ramos-Román et al., 2018b). The spectral analysis was carried out using the PAST 3.19 software (Hammer et al., 2001) with a REDFIT procedure of Schulz and Mudelsee (2002) under the rectangular window function (value of 2 for the segments parameter and value of 3 for the oversample parameter). In order to better observe cyclicities, xerophyte data were filtered under the statistically significant obtained frequencies using the Analyseries 2.0 software (Paillard et al., 1996).

4. Results and discussion

4.1. Chronology of HS1 in southern Europe and the Mediterranean region

The obtained *KDE* ages for the revised, recalibrated and modelled HS1 boundaries of high-resolution records from southern Europe and the Mediterranean region including Padul-15-05 (*KDE Total*) exhibited ages of ~18.0 kyr BP (median value = 17,970 cal yr BP; mean value = 18030 ± 330 cal yr BP) for the onset and ~15.2 kyr BP (median value = 15,210 cal yr BP; mean value = 15200 ± 420 yr) for the end of HS1 (Fig. 3).

The terrestrial paleoclimate record from Padul shows overall cold and arid conditions during HS1, deduced by the decrease in mesic forest and abundance of xerophytes between 18.4 and 15.7 kyr BP (Fig. 4c and d). In addition, the centennial-scale variability observed during HS1 allows for the identification of 3 main climatic phases (i.e., HS1a from 18.4 to 17.2 kyr BP, HS1b from 17.2 to 16.9 kyr BP, and HS1c from 16.9 to 15.7 kyr BP) and a further subdivision in 7 smaller-scale phases within them (i.e., HS1a.1, HS1a.2, HS1a.3, HS1b, HS1c.1, HS1c.2 and HS1c.3) (Fig. 4e and f and Fig. 5a), which are statistically supported by the significance test using the SiZer method (see section 4.2 and Fig. 6).

4.1.1. Three main climatic phases within HS1 from Padul

The three main climatic phases occurring in Padul (HS1a, HS1b and HS1c) have also been observed in marine sediment records from the southern Iberian margin (e.g., U1389 and MD99-2339 sites), described as early, middle and late HS1 phases (Sierro et al., 2020). These oscillations previously observed in the marine sedimentary records were interpreted as consequence of changes in the physicochemical properties of surface water in the Iberian margin.

The first main climatic phase in Padul during HS1 is HS1a (early HS1; 18.4–17.2 kyr BP), characterized by low temperatures with significant variability in precipitation but under generally arid conditions, deduced by high xerophytes and low PCI and *Ip* values (Fig. 4c, e, f). Especially cold/arid conditions during this early phase are confirmed by high Si_{norm} values, which show that high siliciclastic input from the Sierra Nevada range into the wetland are caused by enhanced erosion during decreased forest cover (Camuera et al., 2019). The general cold/arid conditions shown in Padul during the early HS1a were also documented in nearby marine records presenting the 3 main phases for HS1, such as the pollen records from NW Iberia (Naughton et al., 2016), or the pollen data, SST reconstructions (Fig. 5b and c) and foraminifera/coccolithophore assemblages from Alboran Sea (Bazzicalupo et al., 2018; Cacho et al., 1999, 2006; Fletcher and Sánchez Goñi, 2008; Martrat et al., 2014). The early arid HS1a phase recorded in Padul could also

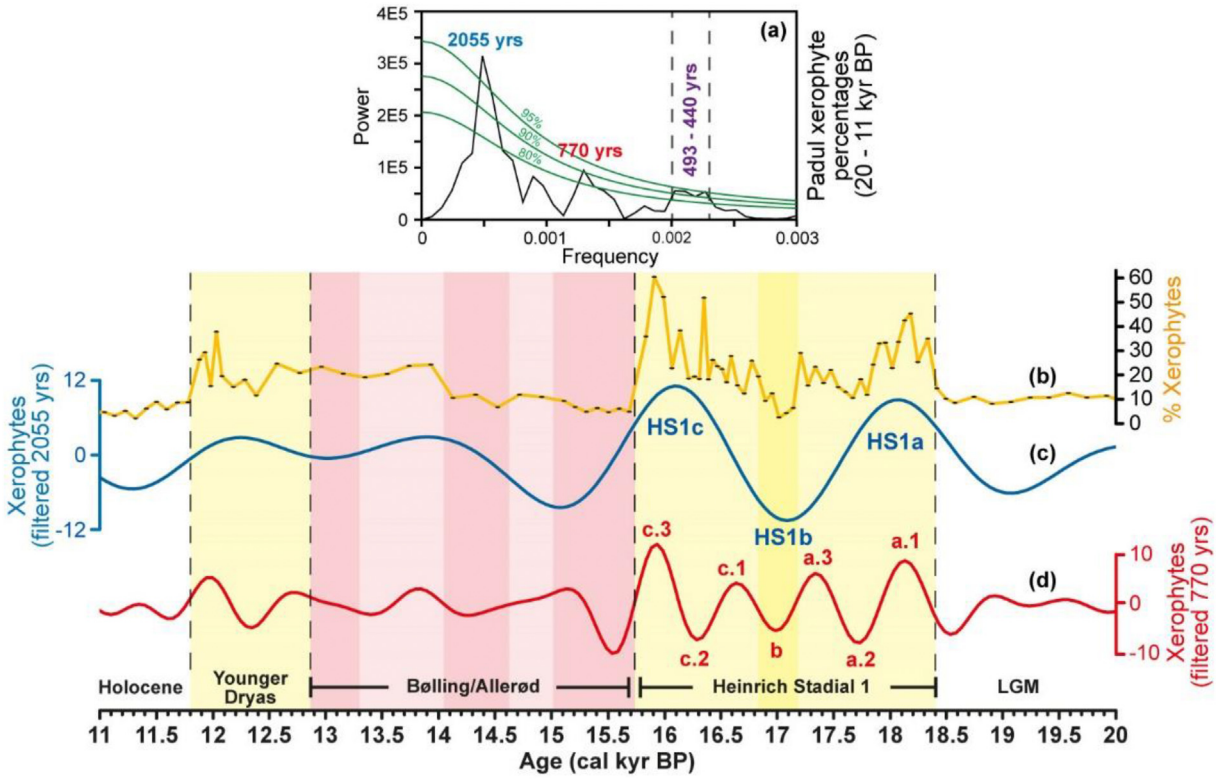

Fig. 7. Cyclostratigraphic analysis of the Padul-15-05 pollen data. (a) Spectral analysis run on Padul xerophyte percentages for the age range between 20 and 11 kyr BP. (b) Percentages of xerophyte taxa from Padul-15-05. (c) Filtered xerophyte data based on the obtained 2055-yr cycle from the spectral analysis (bandwidth parameter of 0.0002). The identified three main phases (HS1a, HS1b and HS1c) within HS1 in Padul are in relation with this ~2000-yr cycle. (d) Filtered xerophyte data based on the 770-yr cycle from the spectral analysis (bandwidth parameter of 0.0005). The internal seven sub-phases (a.1-a.3, b, c.1-c.3) occurring during HS1 in Padul are in relation with this ~800-yr cycle.

be related with the enhancement of the cold Portugal current and the low influence of the Azores Current observed in the marine records by the decrease in $\delta^{18}O$ surface seawater and the low SST (Sierro et al., 2020; Voelker et al., 2009). This cold SST could have produced a slowdown of the thermohaline overturning circulation and decreased of the marine heat transport, resulting in more intense Saharan winds and higher aridity (Jiménez-Espejo et al., 2008; Moreno et al., 2002), as observed in southern Iberian Peninsula and in the Padul record. In addition, the North Atlantic SST also affected the north-westerly wind intensity over Europe and the Mediterranean area, resulting in more arid conditions in the northern Mediterranean region (Moreno et al., 2004).

HS1b (middle HS1; 17.2–16.9 kyr BP) is characterized in Padul by a moderate increase in temperature and precipitation, deduced from low xerophytes, and higher PCI and *Ip* values. This is further supported by low Si_{norm}, indicative of low erosion precluding siliciclastic input in the wetland (Fig. 4b, c, e, f). A similar slightly warmer climate during this phase was recorded in the MD95-2043 (Cacho et al., 1999, 2006) and ODP-976 (Martrat et al., 2014) records from Alboran Sea (Fig. 5b and c; subjected to age uncertainties for onset/ending of HS1). This warmer/wetter conditions agree with increases in temperate forest recorded in the Iberian margin (Daniau et al., 2007), and in runoff in Lake Estanya (NE Spain) (Morellón et al., 2009). This relatively more humid conditions in Padul, could be a result of the higher influence of the Azores Current, observed by the arrival of the warmer SST waters (and higher seawater $\delta^{18}O$) to the Iberian margin (Sierro et al., 2020), also affecting the western Mediterranean Sea (Hodell et al., 2017; Martrat et al., 2014).

HS1c (late HS1; 16.9–15.7 kyr BP) was climatically similar to HS1a, characterized by cold/dry conditions. This is deduced by the observed increase in xerophytes and Si_{norm} and lowering in *Ip* between ~17 and 15.9 kyr BP, related with the decreasing moisture (Fig. 4b, c, e). The general cold/arid climate in Padul during this phase is concordant with low SST from Alboran Sea (Martrat et al., 2014) (Fig. 5b), and with increasing salinity and low lake level in Lake Estanya (see Mystery Interval in Fig. 7 from Morellón et al., 2009). This arid HS1c phase in Padul fits well with the late HS1 identified in the Iberian margin marine records, characterized by cooler and less saline marine water conditions (Sierro et al., 2020). The ice-rafted debris (IRD) H1.1 deposition along the Iberian margin (Eynaud et al., 2009; Voelker et al., 2009) at the beginning of this late phase could have been favored by the southward expansion of subpolar waters, which could have generated the coldest conditions recorded in Padul at ~16.5 kyr BP (Fig. 4f).

4.1.2. Subdivision of HS1 in seven centennial-scale climatic sub-phases in Padul

The high-resolution pollen record from Padul-15-05 with the help of the cluster analysis pollen zonation also revealed shorter centennial-scale climatic variability during HS1a and HS1c with a further climatic subdivision of HS1 into 7 sub-phases. The statistical significance of these sub-phases has been validated by the SiZer test (see section 4.2 below and Fig. 6). The climatic subdivisions of HS1 and the correspondent pollen zones are: HS1a.1 (zone 4 g), HS1a.2 (zone 4f), HS1a.3 (zone 4e), HS1b (zone 4 d), HS1c.1 (zone 4c), HS1c.2 (zone 4 b) and HS1c.3 (zone 4a) (Fig. 4c, e, Fig. 5a and Fig. S3).

HS1a.1 was characterized by a cold/arid phase between 18.4 and 17.8 kyr BP recorded by high xerophytes, and low PCI and *Ip* values. Climate changed towards more humidity in HS1a.2 sub-phase at 17.8–17.5 kyr BP, and returned to enhanced aridity during HS1a.3 between 17.5 and 17.2 kyr BP. This arid-humid-arid climatic pattern is further confirmed by oscillations in Si_{norm} (Fig. 4b, c, e, f and Fig. 5a).

HS1c also presents a three-phase subdivision, namely HS1c.1, HS1c.2 and HS1c.3. HS1c.1 was characterized by a decrease in precipitation and temperature (low *Ip* and lowest PCI values), registering the coldest conditions of HS1 at around 16.5 kyr BP (Fig. 4f). Temperature and moisture conditions increased during HS1c.2 at 16.4–16 kyr BP, whereas similar temperatures but under more arid climate conditions are recorded during HS1c.3 at 16–15.7 kyr BP (Fig. 4c, e, f and Fig. 5a). This arid-humid-arid climatic pattern is similar to the earlier HS1a.

4.2. Significance of the seven climatic sub-phases within HS1 from Padul

A SiZer statistical method was used in this study to test the significance of the internal centennial-scale climate changes occurring during HS1 (Fig. 6).

The first derivative of the 3-point moving average xerophyte data (Fig. 6) shows an increasing trend followed by a decreasing trend between 18.9 and 17.7 kyr BP, coinciding with the concave down function from the second derivative at ~18.2 kyr BP and indicating the first sub-phase of HS1 (HS1a.1). The following concave up (at ~17.7 kyr BP) and the concave down (at ~17.4 kyr BP) functions in the second derivative statistically show the HS1a.2 and HS1a.3 sub-phases, respectively.

The mid phase HS1b is observed by the decreasing-increasing trends in the first derivative between ~17.3 and 16.8 kyr BP and in the concave up feature in the second derivative at ~17 kyr BP.

The HS1c.1 sub-phase is statistically significant looking at the increasing trend in the first derivative between ~17 and 16.4 kyr BP. Although the HS1c.2 sub-phase exhibit a very weak signal, the small concave up function in the second derivative at ~16.2 kyr BP suggests that it is statistically significant. Finally, the last HS1c.3 is statistically well shown by the increasing-decreasing functions in the first derivative between ~16.1 and 15.5 kyr BP and by the concave down function in the second derivative at ~15.9 kyr BP.

4.3. HS1 record in southern Europe and the Mediterranean region

The centennial-scale arid-humid-arid trends recorded during HS1a and HS1c, and the increase in temperature/precipitation during HS1b, are also observed in the SST records from the Alboran Sea in western Mediterranean (Cacho et al., 1999, 2006; Martrat et al., 2014), suggesting a similar response in marine and continental environments (Fig. 5a–c).

However, our study from Padul, supported by the synthetic median ages of the HS1 boundaries obtained with the *KDE* modelling (Fig. 3) shows an early onset and end for HS1 (onset and end in Padul: ~18.4–15.7 kyr BP; *KDE* modelling for the onset and end in southern Europe and the Mediterranean region: ~18–15.2 kyr BP) with respect to the SST records from the Alboran Sea. This asynchronicity could be due to several reasons, including uncertainties in radiocarbon dating. Several previous studies suggested that radiocarbon dating of some specific materials in lacustrine environments (e.g., aquatic organisms) could be affected by a reservoir effect due to "old carbon" dissolved in the hard-water and used by algae and aquatic plants as carbon source (Olsson, 1986; Yu et al., 2007). However, $\delta^{13}C$ and C/N values from the radiocarbon samples used in dating this time interval (Table S1) seem to be in agreement with overall vascular C3 land plants (Meyers, 2003; Meyers and Lallier-vergés, 1999), suggesting a prevailing atmospheric organic carbon source and thus, a reduced or negligible reservoir effect. The age offsets between records could also be related with the significant decrease in the atmospheric ^{14}C between 17.5 and 14.5 kyr, making it difficult to obtain accurate age models based on radiocarbon dating for this time period (Broecker

and Barker, 2007).

The West Antarctic Ice Sheet Divide ice core recorded the beginning of the atmospheric CO_2 rise at 18.1 kyr BP (Marcott et al., 2014), which has been hypothesized to have influence on warming during deglaciation (Denton et al., 2010). The enhanced freshwater discharges from the European ice-sheet at ~18.2 kyr BP (Toucanne et al., 2015) and the meltwater from glaciers in the Alps and Apennines produced the first freshwater input to the western Mediterranean through the large rivers from the northern Mediterranean borderlands at ~19 kyr BP (Bonneau et al., 2014). These processes, along with the large freshwater discharge from the Fennoscandian ice-sheets via the Caspian-Black Sea corridor (Sierro et al., 2020), could have led to the slowdown of the Mediterranean Sea overturning circulation (Fink et al., 2015; Rogerson et al., 2008) and could have produced cold and arid conditions of HS1 in this region, as it is the main factor controlling climate in this area (Rohling et al., 2015).

4.4. Bølling-Allerød (BA) and Younger Dryas (YD)

The BA recorded in Padul between 15.7 and 12.9 kyr BP is characterized by a significant increase in the Mediterranean forest, and thus *Ip* and PCI values. This indicates warmer/wetter climate than during HS1, agreeing with the SST reconstructions from the Alboran Sea (Martrat et al., 2014) (Fig. 5b). In addition, 5 centennial-scale climatic sub-phases were detected during the BA (pollen zones 3e to 3a, Fig. S3) characterized by decreasing temperature and humidity conditions (Fig. 4e and f, Fig. 5a, and Fig. S3).

Cold/arid climate during the YD stadial also affected paleoenvironments in the Padul area between 12.9 and 11.8 kyr BP. The YD is characterized by relatively arid conditions shown by the mean xerophyte percentage of ~22%, similar to the increase in semi-desertic taxa observed in the ODP Leg 161 Site 976 from Alboran Sea (Dormoy et al., 2009). However, temperature seems to increase throughout the YD period, mainly reflected by the increasing trend in the Mediterranean forest (Fig. 4d). Arid conditions during the YD are well marked by a decrease in *Ip* values starting at 12.9 kyr BP. The end of the YD period - the beginning of the Holocene - seems to have occurred at ~11.8 kyr BP, indicated by an increase in the Mediterranean forest, *Ip* and PCI values (Fig. 4c–f).

4.5. Climate variability and solar forcing in the Iberian Peninsula

Centennial- and millennial-scale climate variability have been recorded during HS1, BA and YD periods in Padul. The spectral analysis performed on the xerophytes for the time period between 20 and 11 kyr BP presented periodicities of ~2000 years (frequency (f) = 0.0004865, >95% Confidence Interval (CI)), 800 years (f = 0.001297, >90% CI) and 450 years (f = 0.002270–0.002027, 90–95% CI) (Fig. 7a). In addition, xerophyte data were filtered under the frequencies of the obtained periodicities of ~2000 (f = 0.0004865) and ~800 years (f = 0.001297) (Fig. 7b–d).

These climatic variabilities could be related to solar forcing, as similar cyclicities have been obtained analyzing solar activity with ^{14}C production rates (Damon and Jirikowic, 1992; Turney et al., 2005). Several studies have determined a relation between paleoenvironmental data oscillations linked to climate changes through variations in solar activity (Bond et al., 2001; Lüning and Vahrenholt, 2016). In particular, climate variability during the Last Glacial and Holocene periods was strongly controlled by solar activity, specifically during cold glacial phases, in which solar variability caused larger climate changes (Van Geel et al., 1999) associated to the presence and collapse of ice-sheets (Kawamura et al., 2017). More recent temperature estimations showed that they also seem to be forced by solar variability (Soon et al., 2015). In addition, it has been proved that solar activity changes could affect temperature, air and water masses and thus precipitation on land affecting plants (Lozano-García et al., 2007; Ramos-Román et al., 2016; Tinner and Kaltenrieder, 2005). Kofler et al. (2005) also suggested that solar output caused decreases in pollen production and treeline shifts in the Alps, which could also be affecting vegetation in the Sierra Nevada and, therefore, in the Padul area.

The obtained ~2000-yr climatic cyclicity forced millennial-scale paleoenvironmental variability in Padul and produced the above-mentioned three main phases during HS1: maximum xerophyte values at ~18 (HS1a) and ~16 kyr BP (HS1c), and xerophyte minima at ~17 kyr BP (HS1b) (Fig. 7c). This periodicity could be linked with the previously described suborbital 1–2 kyr climate variability recorded during the last glaciation, such as the ~1.8-kyr cycle identified on the hematite-stained grain record from North Atlantic cores (Bond et al., 1999). Paleoclimatic records from the Equator and Southern Hemisphere also determined periodic surface temperature variations of around 2000 yrs in relation with solar irradiance (Bütikofer, 2007). This 2000-yr cycles are pervasive for the last 20 kyr BP, at least in Southern Iberia, associated to solar activity and/or monsoon-like activity (Rodrigo-Gámiz et al., 2014). Subsequent studies demonstrate that this monsoon-like signal is linked to Nile input (Bahr et al., 2015), transmitted by Mediterranean thermohaline circulation to western Europe (Kaboth-Bahr et al., 2018) and associated with winter precipitation for the last 1.3 Myr in Southern European lacustrine records (Wagner et al., 2019).

The ~800-yr cycle identified in Padul forced the 7 centennial-scale climatic sub-phases subdivision of HS1. This cyclicity explains the maximum xerophyte values at ~18.2, 17.3, 16.5 and 15.8 kyr BP (HS1a.1, HS1a.3, HS1c.1 and HS1c.3 sub-phases, respectively) and xerophyte minima at ~17.7, 17 and 16.1 kyr BP (HS1a.2, HS1b and HS1c.2) (Fig. 7d). Other global paleoclimatic studies also show similar frequencies caused by solar variability. For example, an ~800-yr cycle was observed in Irish oak tree chronologies (Turney et al., 2005) and in Mg/Ca SST from the Pacific Ocean (Marchitto et al., 2010), both records closely related to solar irradiance. A 890-yr cycle was also found in the $\delta^{18}O$ GISP2 Holocene time series from Greenland and interpreted as linked to solar radiation (Schulz and Paul, 2002). Consequently, the ~800-yr cycle detected in Padul and in other worldwide records suggests a linkage between centennial-scale paleoenvironmental changes and solar activity.

Despite the age offsets between Padul and Alboran SST records (Fig. 5a–c) due to possible reasons explained above (see section 4.3), this study shows that similar centennial-scale oscillations have been regionally recorded in both environments during HS1, suggesting a close land-sea relationship in response to solar variability. The Mediterranean SST could have been affected by solar activity, similar to the North Atlantic cooling episodes linked to reduced solar irradiance (Bond et al., 2001). In addition, observed variations in the Padul data suggest a southward shift of the North Atlantic polar front during HS1 (Repschläger et al., 2015), which could have produced a penetration of colder Atlantic surface waters into the Mediterranean (Cacho et al., 1999; Jiménez-Espejo et al., 2008; Sierro et al., 2005, 2020). These conditions, along with the southward displacement of the North Atlantic atmospheric polar front, could have produced a low land-sea temperature contrast and weak moisture advection between both environments, and therefore, increasing aridity in the western Mediterranean during cold sub-phases HS1a.1, HS1a.3, HS1c.1 and HS1c.3. Similar conditions linked to weak moisture advection were interpreted in the eastern Mediterranean during HS1 and HS2 (Kwiecien et al., 2009) and in the Corchia Cave during HS11 (Drysdale et al., 2009). In contrast, during warmer sub-phases in Padul (i.e., HS1a.2, HS1b and HS1c.2) and in Mediterranean SSTs, enhanced marine evaporation and moisture advection toward the continent could have provoked

wetter climate conditions in southern Iberian Peninsula.

5. Conclusions

The high-resolution study of the Padul-15-05 record for the 20–11 kyr BP interval, together with other twenty non-tuned and independently-dated paleoclimatic records from 16 sites documenting HS1 in southern Europe and the Mediterranean region show that:

1) The synthetic median ages for the onset and the end of HS1 based on the recalibration and the *KDE* age-modelling of the HS1 boundaries of the non-tuned and independently-dated marine and terrestrial records from this area are ~18.0 kyr BP (exact median age = 17,970 cal yr BP; mean age = 18,030 ± 330 cal yr BP) and ~15.2 kyr BP (exact median age = 15,210 cal yr BP; mean age = 15,200 ± 420 cal yr BP), respectively. Several environmental conditions and causes have been suggested for this delimitation of HS1 age-range, including uncertainties in radiocarbon dating, the warming during deglaciation caused by the CO_2 rise and/or the slowdown of the Mediterranean Sea overturning circulation result of the European ice-sheets and alpine glacier retreats and subsequent meltwater input into the Mediterranean.
2) Centennial-scale climate oscillations affected southern Iberian Peninsula during HS1, with three main phases HS1a (18.4–17.2 kyr BP), HS1b (17.2–16.9 kyr BP) and HS1c (16.9–15.7 kyr BP) characterized by general arid (cold), more humid (cool) and arid (cold) climate, respectively. Similar climatic phases during HS1 have also been observed in marine records from the Alboran Sea, suggesting a good relationship between the ocean dynamics and atmospheric conditions in the western Mediterranean.
3) We suggest, for the first time, a further subdivision within these 3 main climatic phases of HS1 in 7 sub-phases: 3 sub-phases (a.1-a.3) during HS1a, HS1b, and 3 sub-phases (c.1-c.3) during HS1c. The statistically confirmed climatic variability from Padul is also identified in western Mediterranean SST records, confirming this climatic pattern at regional-scale.
4) The main periodicities obtained for climatic oscillations of ~2000 and ~800 yrs for the time period between 20 and 11 kyr BP seem to be related to solar forcing. Variations in solar activity could have influenced latitudinal shifts of the North Atlantic and atmospheric polar fronts, affecting the land-sea temperature contrast, marine evaporation and moisture advection toward the continent.

Declaration of competing interest

The authors declare that they have no known competing financial interests or personal relationships that could have appeared to influence the work reported in this paper.

Acknowledgments

This research is supported by the projects CGL 2013-47038-R and CGL-2017-85415-R, B-RNM-144-UGR18, PhD funding BES-2014-069117 (J.C.) and Ramón y Cajal fellowship RYC-2015-18966 (A.G.-A.) provided by the Ministerio de Economía y Competitividad of the Spanish Government. Additional funding was provided by the project number 316702 from the Academy of Finland for a postdoctoral research contract (J.C.) and the research group RNM0190 and the project P11-RNM-7332 with a postdoctoral fellowship (M.J.R.-R.) from the Junta de Andalucía. M.J.R.-R. acknowledges the postdoctoral funding provided by the European Commission/H2020 (ERC-2017-ADG, project number 788616). Finally, we acknowledge two anonymous reviewers and the editor (Donatella Magri) for their very useful corrections and suggestions.

Appendix A. Supplementary data

Supplementary data to this article can be found online at https://doi.org/10.1016/j.quascirev.2021.106814.

Data availability

The paleoclimatic pollen data from Padul-15-05 can be found in the PANGAEA data repository (https://doi.pangaea.de/10.1594/PANGAEA.904053).

Author statement

Jon Camuera performed the pollen, XRF and spectral analyses, interpreted the data and wrote the manuscript. Gonzalo Jiménez-Moreno discussed data and interpretations and wrote the manuscript. María José Ramos-Román. performed the XRF analysis, discussed data and interpretations and contributed to the writing of the manuscript. Antonio García-Alix., Jaime L. Toney, R. Scott Anderson, Francisco J. Jiménez-Espejo and Cole Webster discussed data and interpretations and contributed to the writing of the manuscript.

References

AEMET, 2016. Agencia Estatal de Meteorología, Visor del Atlas climático de la Península y Baleares, pp. 1971–2000. http://agroclimap.aemet.es.

Bahr, A., Kaboth, S., Jiménez-Espejo, F.J., Sierro, F.J., Voelker, A.H.L., Lourens, L., Röhl, U., Reichart, G.J., Escutia, C., Hernández-Molina, F.J., Pross, J., Friedrich, O., 2015. Persistent monsoonal forcing of mediterranean outflow water dynamics during the late Pleistocene. Geology 43, 951–954. https://doi.org/10.1130/g37013.1.

Barker, S., Diz, P., Vautravers, M.J., Pike, J., Knorr, G., Hall, I.R., Broecker, W.S., 2009. Interhemispheric Atlantic seesaw response during the last deglaciation. Nature 457, 1097–1102. https://doi.org/10.1038/nature07770.

Bazzicalupo, P., Maiorano, P., Girone, A., Marino, M., Combourieu-Nebout, N., Incarbona, A., 2018. High-frequency climate fluctuations over the last deglaciation in the Alboran Sea, Western Mediterranean: evidence from calcareous plankton assemblages. Palaeogeogr. Palaeoclimatol. Palaeoecol. 506, 226–241. https://doi.org/10.1016/j.palaeo.2018.06.042.

Bertini, A., Toti, F., Marino, M., Ciaranfi, N., 2015. Vegetation and climate across the early–middle Pleistocene transition at montalbano jonico, southern Italy. Quat. Int. 383, 74–88. https://doi.org/10.1016/j.quaint.2015.01.003.

Blaauw, M., Christen, J.A., 2011. Flexible paleoclimate age-depth models using an autoregressive gamma process. Bayesian Anal 6, 457–474. https://doi.org/10.1214/11-BA618.

Bond, G., Broecker, W., Johnsen, S., McManus, J., Labeyrie, L., Jouzel, J., Bonani, G., 1993. Correlations between climate records from North Atlantic sediments and Greenland ice. Nature 365, 143. https://doi.org/10.1038/365143a0.

Bond, G., Kromer, B., Beer, J., Muscheler, R., Evans, M.N., Showers, W., Hoffmann, S., Lotti-Bond, R., Hajdas, I., Bonani, G., 2001. Persistent solar influence on North Atlantic climate during the Holocene. Science 294, 2130–2136. https://doi.org/10.1126/science.1065680.

Bond, G.C., Showers, W., Elliot, M., Evans, M., Lotti, R., Hajdas, I., Bonani, G., Johnson, S., 1999. the North atlantic's 1-2 kyr climate rhythm: relation to Heinrich events, dansgaard/oeschger cycles and the little ice age. Mechanisms of global climate change at millennial time scales 112, 35–58. https://doi.org/10.1029/GM112p0035.

Bonneau, L., Jorry, S.J., Toucanne, S., Silva Jacinto, R., Emmanuel, L., 2014. Millennial-scale response of a western Mediterranean river to late Quaternary climate changes: a view from the deep sea. J. Geol. 122, 687–703. https://doi.org/10.1086/677844.

Bouimetarhan, I., Prange, M., Schefuß, E., Dupont, L., Lippold, J., Mulitza, S., Zonneveld, K., 2012. Sahel megadrought during Heinrich Stadial 1: evidence for a three-phase evolution of the low- and mid-level West African wind system. Quat. Sci. Rev. 58, 66–76. https://doi.org/10.1016/j.quascirev.2012.10.015.

Broecker, W., Barker, S., 2007. A 190‰ drop in atmosphere's Δ14C during the "Mystery Interval"(17.5 to 14.5 kyr). Earth Planet Sci. Lett. 256, 90–99. https://doi.org/10.1016/j.epsl.2007.01.015.

Brooks, S.P., Gelman, A., 1998. General methods for monitoring convergence of iterative simulations. J. Comput. Graph Stat. 7, 434–455. https://doi.org/10.1080/10618600.1998.10474787.

Bütikofer, J., 2007. Millennial Scale Climate Variability during the Last 6000 Years—Tracking Down the Bond Cycles. University of Bern, p. 124.
Cacho, I., Grimalt, J.O., Pelejero, C., Canals, M., Sierro, F.J., Flores, J.A., Shackleton, N., 1999. Dansgaard-oeschger and Heinrich event imprints in Alboran Sea paleotemperatures. Paleoceanography 14, 698—705. https://doi.org/10.1029/1999PA900044.
Cacho, I., Shackleton, N., Elderfield, H., Sierro, F.J., Grimalt, J.O., 2006. Glacial rapid variability in deep-water temperature and δ18O from the Western Mediterranean Sea. Quat. Sci. Rev. 25, 3294—3311. https://doi.org/10.1016/j.quascirev.2006.10.004.
Camuera, J., Jiménez-Moreno, G., Ramos-Román, M.J., García-Alix, A., Toney, J.L., Anderson, R.S., Jiménez-Espejo, F., Bright, J., Webster, C., Yanes, Y., 2019. Vegetation and climate changes during the last two glacial-interglacial cycles in the western Mediterranean: a new long pollen record from Padul (southern Iberian Peninsula). Quat. Sci. Rev. 205, 86—105. https://doi.org/10.1016/j.quascirev.2018.12.013.
Camuera, J., Jiménez-Moreno, G., Ramos-Román, M.J., García-Alix, A., Toney, J.L., Anderson, R.S., Jiménez-Espejo, F., Kaufman, D., Bright, J., Webster, C., 2018. Orbital-scale environmental and climatic changes recorded in a new ~ 200,000-year-long multiproxy sedimentary record from Padul, southern Iberian Peninsula. Quat. Sci. Rev. 198, 91—114. https://doi.org/10.1016/j.quascirev.2018.08.014.
Castañeda, I.S., Schouten, S., Pätzold, J., Lucassen, F., Kasemann, S., Kuhlmann, H., Schefuß, E., 2016. Hydroclimate variability in the Nile River basin during the past 28,000 years. Earth Planet Sci. Lett. 438, 47—56. https://doi.org/10.1016/j.epsl.2015.12.014.
Chaudhuri, P., Marron, J.S., 1999. SiZer for Exploration of Structures in Curves. Journal of the American Statistical Association 94, 807—823. https://doi.org/10.1080/01621459.1999.10474186.
Combourieu Nebout, N., Londeix, L., Baudin, F., Turon, J.-L., Von Grafenstein, R., Zahn, R., 1999. Quaternary marine and continental paleoenvironments in the western Mediterranean (Site 976, Alboran Sea): palynological evidence. In: Proceedings of the Ocean Drilling Program. Scientific Results. Ocean Drilling Program, pp. 457—468.
Damon, P.E., Jirikowic, J.L., 1992. The sun as a low-frequency harmonic oscillator. Radiocarbon 34, 199—205. https://doi.org/10.1017/S003382220001362X.
Daniau, A.-L., Sánchez-Goñi, M., Beaufort, L., Laggoun-Défarge, F., Loutre, M.-F., Duprat, J., 2007. Dansgaard—Oeschger climatic variability revealed by fire emissions in southwestern Iberia. Quat. Sci. Rev. 26, 1369—1383. https://doi.org/10.1016/j.quascirev.2007.02.005.
Denton, G.H., Anderson, R.F., Toggweiler, J.R., Edwards, R.L., Schaefer, J.M., Putnam, A.E., 2010. The Last Glacial Termination. Science 328, 1652—1656. https://doi.org/10.1126/science.1184119.
Dormoy, I., Peyron, O., Combourieu Nebout, N., Goring, S., Kotthoff, U., Magny, M., Pross, J., 2009. Terrestrial climate variability and seasonality changes in the Mediterranean region between 15 000 and 4000 years BP deduced from marine pollen records. Clim. Past 5, 615—632. https://doi.org/10.5194/cp-5-615-2009.
Drysdale, R., Hellstrom, J., Zanchetta, G., Fallick, A., Goñi, M.S., Couchoud, I., McDonald, J., Maas, R., Lohmann, G., Isola, I., 2009. Evidence for obliquity forcing of glacial termination II. Science 325, 1527—1531. https://doi.org/10.1126/science.1170371.
Dupont, L.M., Schlütz, F., Ewah, C.T., Jennerjahn, T.C., Paul, A., Behling, H., 2010. Two-step vegetation response to enhanced precipitation in Northeast Brazil during Heinrich event 1. Global Change Biol. 16, 1647—1660. https://doi.org/10.1111/j.1365-2486.2009.02023.x.
Escobar, J., Hodell, D.A., Brenner, M., Curtis, J.H., Gilli, A., Mueller, A.D., Anselmetti, F.S., Ariztegui, D., Grzesik, D.A., Pérez, L., Schwalb, A., Guilderson, T.P., 2012. A ~43-ka record of paleoenvironmental change in the Central American lowlands inferred from stable isotopes of lacustrine ostracods. Quat. Sci. Rev. 37, 92—104. https://doi.org/10.1016/j.quascirev.2012.01.020.
Eynaud, F., De Abreu, L., Voelker, A., Schönfeld, J., Salgueiro, E., Turon, J.L., Penaud, A., Toucanne, S., Naughton, F., Sánchez Goñi, M.F., 2009. Position of the Polar Front along the western Iberian margin during key cold episodes of the last 45 ka. Geochem. Geophys. Geosyst. 10 https://doi.org/10.1029/2009GC002398.
Faegri, K., Iversen, J., 1989. Textbook of Pollen Analysis, fourth ed. Wiley, New York.
Fan, J., Gijbels, I., 1996. Local polynomial modelling and its applications: monographs on statistics and applied probability 66. CRC Press.
Fernández-López de Pablo, J., Gutiérrez-Roig, M., Gómez-Puche, M., McLaughlin, R., Silva, F., Lozano, S., 2019. Palaeodemographic modelling supports a population bottleneck during the Pleistocene-Holocene transition in Iberia. Nat. Commun. 10, 1872. https://doi.org/10.1038/s41467-019-09833-3.
Fink, H.G., Wienberg, C., De Pol-Holz, R., Hebbeln, D., 2015. Spatio-temporal distribution patterns of Mediterranean cold-water corals (Lophelia pertusa and Madrepora oculata) during the past 14,000 years. Deep Sea Res. Oceanogr. Res. Pap. 103, 37—48. https://doi.org/10.1016/j.dsr.2015.05.006.
Fletcher, W.J., Sánchez Goñi, M.F., 2008. Orbital- and sub-orbital-scale climate impacts on vegetation of the western Mediterranean basin over the last 48,000 yr. Quat. Res. 70, 451—464. https://doi.org/10.1016/j.yqres.2008.07.002.
Fletcher, W.J., Sánchez Goñi, M.F., Allen, J.R.M., Cheddadi, R., Combourieu-Nebout, N., Huntley, B., Lawson, I., Londeix, L., Magri, D., Margari, V., Müller, U.C., Naughton, F., Novenko, E., Roucoux, K., Tzedakis, P.C., 2010a. Millennial-scale variability during the last glacial in vegetation records from Europe. Quat. Sci. Rev. 29, 2839—2864. https://doi.org/10.1016/j.quascirev.2009.11.015.
Fletcher, W.J., Sánchez Goñi, M.F., Peyron, O., Dormoy, I., 2010b. Abrupt climate changes of the last deglaciation detected in a Western Mediterranean forest record. Clim. Past 6, 245—264. https://doi.org/10.5194/cp-6-245-2010.
García-Antón, M., Franco-Múgica, F., Morla-Juaristi, C., Maldonado-Ruiz, J., 2011. The biogeographical role of Pinus forest on the Northern Spanish Meseta: a new Holocene sequence. Quat. Sci. Rev. 30, 757—768. https://doi.org/10.1016/j.quascirev.2010.12.023.
Giesche, A., Staubwasser, M., Petrie, C., Hodell, D., 2019. Indian winter and summer monsoon strength over the 4.2 ka BP event in foraminifer isotope records from the Indus River delta in the Arabian Sea. Clim. Past 15, 73—90. https://doi.org/10.5194/cp-15-73-2019.
Grimm, E.C., 1987. CONISS: a FORTRAN 77 program for stratigraphically constrained cluster analysis by the method of incremental sum of squares. Comput. Geosci. 13, 13—35. https://doi.org/10.1016/0098-3004(87)90022-7.
Hald, M., Ebbesen, H., Forwick, M., Godtliebsen, F., Khomenko, L., Korsun, S., Ringstad Olsen, L., Vorren, T.O., 2004. Holocene paleoceanography and glacial history of the West Spitsbergen area, Euro-Arctic margin. Quat. Sci. Rev. 23, 2075—2088. https://doi.org/10.1016/j.quascirev.2004.08.006.
Hammer, Ø., Harper, D., Ryan, P., 2001. PAST-palaeontological Statistics, vol. 25.
Heinrich, H., 1988. Origin and consequences of cyclic ice rafting in the northeast Atlantic Ocean during the past 130,000 years. Quat. Res. 29, 142—152. https://doi.org/10.1016/0033-5894(88)90057-9.
Hemming, S.R., 2004. Heinrich events: massive late Pleistocene detritus layers of the North Atlantic and their global climate imprint. Rev. Geophys. 42 https://doi.org/10.1029/2003RG000128.
Höbig, N., Weber, M.E., Kehl, M., Weniger, G.-C., Julià, R., Melles, M., Fülöp, R.-H., Vogel, H., Reicherter, K., 2012. Lake Banyoles (northeastern Spain): a Last Glacial to Holocene multi-proxy study with regard to environmental variability and human occupation. Quat. Int. 274, 205—218. https://doi.org/10.1016/j.quaint.2012.05.036.
Hodell, D.A., Nicholl, J.A., Bontognali, T.R., Danino, S., Dorador, J., Dowdeswell, J.A., Einsle, J., Kuhlmann, H., Martrat, B., Mleneck-Vautravers, M.J., 2017. Anatomy of Heinrich layer 1 and its role in the last deglaciation. Paleoceanography 32, 284—303. https://doi.org/10.1002/2016PA003028.
Jiménez-Espejo, F., Martínez-Ruiz, F., Rogerson, M., González-Donoso, J., Romero, O., Linares, D., Sakamoto, T., Gallego-Torres, D., Rueda Ruiz, J., Ortega-Huertas, M., 2008. Detrital input, productivity fluctuations, and water mass circulation in the westernmost Mediterranean Sea since the Last Glacial Maximum. Geochem. Geophys. Geosyst. 9 https://doi.org/10.1029/2008GC002096.
Jiménez-Moreno, G., Anderson, R.S., 2012. Holocene vegetation and climate change recorded in alpine bog sediments from the Borreguiles de la Virgen, Sierra Nevada, southern Spain. Quat. Res. 77, 44—53. https://doi.org/10.1016/j.yqres.2011.09.006.
Joannin, S., Bassinot, F., Nebout, N.C., Peyron, O., Beaudouin, C., 2011. Vegetation response to obliquity and precession forcing during the Mid-Pleistocene Transition in Western Mediterranean region (ODP site 976). Quat. Sci. Rev. 30, 280—297. https://doi.org/10.1016/j.quascirev.2010.11.009.
Kaboth-Bahr, S., Bahr, A., Zeeden, C., Toucanne, S., Eynaud, F., Jiménez-Espejo, F., Röhl, U., Friedrich, O., Pross, J., Löwemark, L., Lourens, L.J., 2018. Monsoonal forcing of European ice-sheet dynamics during the late quaternary. Geophys. Res. Lett. https://doi.org/10.1029/2018gl078751.
Kawamura, K., Abe-Ouchi, A., Motoyama, H., Ageta, Y., Aoki, S., Azuma, N., Fujii, Y., Fujita, K., Fujita, S., Fukui, K., Furukawa, T., Furusaki, A., Goto-Azuma, K., Greve, R., Hirabayashi, M., Hondoh, T., Hori, A., Horikawa, S., Horiuchi, K., Igarashi, M., Iizuka, Y., Kameda, T., Kanda, H., Kohno, M., Kuramoto, T., Matsushi, Y., Miyahara, M., Miyake, T., Miyamoto, A., Nagashima, Y., Nakayama, Y., Nakazawa, T., Nakazawa, F., Nishio, F., Obinata, I., Ohgaito, R., Oka, A., Okuno, J.i., Okuyama, J., Oyabu, I., Parrenin, F., Pattyn, F., Saito, F., Saito, T., Saito, T., Sakurai, T., Sasa, K., Seddik, H., Shibata, Y., Shinbori, K., Suzuki, K., Suzuki, T., Takahashi, A., Takahashi, K., Takahashi, S., Takata, M., Tanaka, Y., Uemura, R., Watanabe, G., Watanabe, O., Yamasaki, T., Yokoyama, K., Yoshimori, M., Yoshimoto, T., 2017. State dependence of climatic instability over the past 720,000 years from Antarctic ice cores and climate modeling. Science Advances 3, e1600446. https://doi.org/10.1126/sciadv.1600446.
Kofler, W., Krapf, V., Oberhuber, W., Bortenschlager, S., 2005. Vegetation responses to the 8200 cal. BP cold event and to long-term climatic changes in the Eastern Alps: possible influence of solar activity and North Atlantic freshwater pulses. Holocene 15, 779—788. https://doi.org/10.1191/0959683605hl852ft.
Kwiecien, O., Arz, H.W., Lamy, F., Plessen, B., Bahr, A., Haug, G.H., 2009. North Atlantic control on precipitation pattern in the eastern Mediterranean/Black Sea region during the last glacial. Quat. Res. 71, 375—384. https://doi.org/10.1016/j.yqres.2008.12.004.
Lionello, P., 2012. The Climate of the Mediterranean Region: from the Past to the Future. Elsevier.
Lozano-García, M.d.S., Caballero, M., Ortega, B., Rodríguez, A., Sosa, S., 2007. Tracing the effects of the little ice age in the tropical lowlands of eastern mesoamerica. Proc. Natl. Acad. Sci. Unit. States Am. 104, 16200. https://doi.org/10.1073/pnas.0707896104.
Lüning, S., Vahrenholt, F., 2016. Chapter 16 - the sun's role in climate. In: Easterbrook, D.J. (Ed.), Evidence-Based Climate Science, second ed. Elsevier, pp. 283—305.
Marchitto, T.M., Muscheler, R., Ortiz, J.D., Carriquiry, J.D., van Geen, A., 2010. Dynamical response of the tropical Pacific Ocean to solar forcing during the early Holocene. Science 330, 1378—1381. https://doi.org/10.1126/science.1194887.
Marcott, S.A., Bauska, T.K., Buizert, C., Steig, E.J., Rosen, J.L., Cuffey, K.M., Fudge, T.J., Severinghaus, J.P., Ahn, J., Kalk, M.L., McConnell, J.R., Sowers, T., Taylor, K.C., White, J.W.C., Brook, E.J., 2014. Centennial-scale changes in the global carbon

cycle during the last deglaciation. Nature 514, 616–619. https://doi.org/10.1038/nature13799.
Martrat, B., Grimalt, J.O., Lopez-Martinez, C., Cacho, I., Sierro, F.J., Flores, J.A., Zahn, R., Canals, M., Curtis, J.H., Hodell, D.A., 2004. Abrupt temperature changes in the Western Mediterranean over the past 250,000 years. Science 306, 1762–1765. https://doi.org/10.1126/science.1101706.
Martrat, B., Grimalt, J.O., Shackleton, N.J., de Abreu, L., Hutterli, M.A., Stocker, T.F., 2007. Four climate cycles of recurring deep and surface water destabilizations on the Iberian margin. Science 317, 502–507. https://doi.org/10.1126/science.1139994.
Martrat, B., Jimenez-Amat, P., Zahn, R., Grimalt, J.O., 2014. Similarities and dissimilarities between the last two deglaciations and interglaciations in the North Atlantic region. Quat. Sci. Rev. 99, 122–134. https://doi.org/10.1016/j.quascirev.2014.06.016.
McManus, J.F., Francois, R., Gherardl, J.M., Kelgwin, L., Drown-Leger, S., 2004. Collapse and rapid resumption of Atlantic meridional circulation linked to deglacial climate changes. Nature 428, 834–837. https://doi.org/10.1038/nature02494.
Meyers, P.A., 2003. Applications of organic geochemistry to paleolimnological reconstructions: a summary of examples from the Laurentian Great Lakes. Org. Geochem. 34, 261–289. https://doi.org/10.1016/S0146-6380(02)00168-7.
Meyers, P.A., Lallier-vergés, E., 1999. Lacustrine sedimentary organic matter records of late quaternary paleoclimates. J. Paleolimnol. 21, 345–372. https://doi.org/10.1023/A:1008073732192.
Morales-Molino, C., Postigo-Mijarra, J.M., Morla, C., García-Antón, M., 2011. Long-term persistence of mediterranean pine forests in the duero basin (central Spain) during the Holocene: the case of Pinus pinaster aiton. Holocene 22, 561–570. https://doi.org/10.1177/0959683611427339.
Morellón, M., Valero-Garcés, B., Vegas-Vilarrúbia, T., González-Sampériz, P., Romero, Ó., Delgado-Huertas, A., Mata, P., Moreno, A., Rico, M., Corella, J.P., 2009. Lateglacial and Holocene palaeohydrology in the western mediterranean region: the Lake Estanya record (NE Spain). Quat. Sci. Rev. 28, 2582–2599. https://doi.org/10.1016/j.quascirev.2009.05.014.
Moreno, A., Cacho, I., Canals, M., Grimalt, J.O., Sanchez-Vidal, A., 2004. Millennial-scale variability in the productivity signal from the Alboran Sea record, Western Mediterranean Sea. Palaeogeogr. Palaeoclimatol. Palaeoecol. 211, 205–219. https://doi.org/10.1016/j.palaeo.2004.05.007.
Moreno, A., Cacho, I., Canals, M., Prins, M.A., Sánchez-Goni, M.F., Grimalt, J.O., Weltje, G.J., 2002. Saharan dust transport and high-latitude glacial climatic variability: The Alboran Sea record. Quat. Res. 58, 318–328. https://doi.org/10.1006/qres.2002.2383.
Moreno, A., Stoll, H., Jiménez-Sánchez, M., Cacho, I., Valero-Garcés, B., Ito, E., Edwards, R.L., 2010. A speleothem record of glacial (25–11.6kyr BP) rapid climatic changes from northern Iberian Peninsula. Global Planet. Change 71, 218–231. https://doi.org/10.1016/j.gloplacha.2009.10.002.
Naughton, F., Sanchez Goñi, M.F., Kageyama, M., Bard, E., Duprat, J., Cortijo, E., Desprat, S., Malaizé, B., Joly, C., Rostek, F., 2009. Wet to dry climatic trend in north-western Iberia within Heinrich events. Earth Planet Sci. Lett. 284, 329–342. https://doi.org/10.1016/j.epsl.2009.05.001.
Naughton, F., Sanchez Goñi, M.F., Rodrigues, T., Salgueiro, E., Costas, S., Desprat, S., Duprat, J., Michel, E., Rossignol, L., Zaragosi, S., Voelker, A.H.L., Abrantes, F., 2016. Climate variability across the last deglaciation in NW Iberia and its margin. Quat. Int. 414, 9–22. https://doi.org/10.1016/j.quaint.2015.08.073.
Olsson, I.U., 1986. A study of errors in 14C dates of peat and sediment. Radiocarbon 28, 429–435. https://doi.org/10.1017/S0033822200007554.
Ortiz, J.E., Torres, T., Delgado, A., Julià, R., Lucini, M., Llamas, F.J., Reyes, E., Soler, V., Valle, M., 2004. The palaeoenvironmental and palaeohydrological evolution of Padul Peat Bog (Granada, Spain) over one million years, from elemental, isotopic and molecular organic geochemical proxies. Org. Geochem. 35, 1243–1260. https://doi.org/10.1016/j.orggeochem.2004.05.013.
Paillard, D., Labeyrie, L., Yiou, P., 1996. Macintosh program performs time-series analysis. Eos, Transactions American Geophysical Union 77. https://doi.org/10.1029/96EO00259, 379-379.
Panagiotopoulos, K., Böhm, A., Leng, M.J., Wagner, B., Schäbitz, F., 2014. Climate variability over the last 92 ka in SW Balkans from analysis of sediments from Lake Prespa. Clim. Past 10, 643–660. https://doi.org/10.5194/cp-10-643-2014.
Pini, R., Ravazzi, C., Donegana, M., 2009. Pollen stratigraphy, vegetation and climate history of the last 215ka in the Azzano Decimo core (plain of Friuli, north-eastern Italy). Quat. Sci. Rev. 28, 1268–1290. https://doi.org/10.1016/j.quascirev.2008.12.017.
Ramos-Román, M.J., Jiménez-Moreno, G., Anderson, R.S., García-Alix, A., Toney, J.L., Jiménez-Espejo, F.J., Carrión, J.S., 2016. Centennial-scale vegetation and North Atlantic oscillation changes during the late Holocene in the southern Iberia. Quat. Sci. Rev. 143, 84–95. https://doi.org/10.1016/j.quascirev.2016.05.007.
Ramos-Román, M.J., Jiménez-Moreno, G., Camuera, J., García-Alix, A., Anderson, R.S., Jiménez-Espejo, F.J., Carrión, J.S., 2018a. Holocene climate aridification trend and human impact interrupted by millennial- and centennial-scale climate fluctuations from a new sedimentary record from Padul (Sierra Nevada, southern Iberian Peninsula). Clim. Past 14, 117–137. https://doi.org/10.5194/cp-14-117-2018.
Ramos-Román, M.J., Jiménez-Moreno, G., Camuera, J., García-Alix, A., Scott Anderson, R., Jiménez-Espejo, F.J., Sachse, D., Toney, J.L., Carrión, J.S., Webster, C., Yanes, Y., 2018b. Millennial-scale cyclical environment and climate variability during the Holocene in the western Mediterranean region deduced from a new multi-proxy analysis from the Padul record (Sierra Nevada, Spain). Global Planet. Change 168, 35–53. https://doi.org/10.1016/j.gloplacha.2018.06.003.
Ramsey, C.B., 2017. Methods for summarizing radiocarbon datasets. Radiocarbon 59, 1809–1833. https://doi.org/10.1017/RDC.2017.108.
Rasmussen, S.O., Bigler, M., Blockley, S.P., Blunier, T., Buchardt, S.L., Clausen, H.B., Cvijanovic, I., Dahl-Jensen, D., Johnsen, S.J., Fischer, H., Gkinis, V., Guillevic, M., Hoek, W.Z., Lowe, J.J., Pedro, J.B., Popp, T., Seierstad, I.K., Steffensen, J.P., Svensson, A.M., Vallelonga, P., Vinther, B.M., Walker, M.J.C., Wheatley, J.J., Winstrup, M., 2014. A stratigraphic framework for abrupt climatic changes during the Last Glacial period based on three synchronized Greenland ice-core records: refining and extending the INTIMATE event stratigraphy. Quat. Sci. Rev. 106, 14–28. https://doi.org/10.1016/j.quascirev.2014.09.007.
Repschläger, J., Weinelt, M., Kinkel, H., Andersen, N., Garbe-Schönberg, D., Schwab, C., 2015. Response of the subtropical North Atlantic surface hydrography on deglacial and Holocene AMOC changes. Paleoceanography 30, 456–476. https://doi.org/10.1002/2014pa002637.
Rodrigo-Gámiz, M., Martínez-Ruiz, F., Rodríguez-Tovar, F.J., Jiménez-Espejo, F.J., Pardo-Igúzquiza, E., 2014. Millennial- to centennial-scale climate periodicities and forcing mechanisms in the westernmost Mediterranean for the past 20,000 yr. Quat. Res. 81, 78–93. https://doi.org/10.1016/j.yqres.2013.10.009.
Rogerson, M., Cacho, I., Jimenez-Espejo, F., Reguera, M.I., Sierro, F.J., Martinez-Ruiz, F., Frigola, J., Canals, M., 2008. A dynamic explanation for the origin of the western Mediterranean organic-rich layers. Geochem. Geophys. Geosyst. 9 https://doi.org/10.1029/2007GC001936.
Rohling, E., Marino, G., Grant, K., 2015. Mediterranean climate and oceanography, and the periodic development of anoxic events (sapropels). Earth Sci. Rev. 143, 62–97. https://doi.org/10.1016/j.earscirev.2015.01.008.
Salgueiro, E., Naughton, F., Voelker, A.H.L., de Abreu, L., Alberto, A., Rossignol, L., Duprat, J., Magalhães, V.H., Vaqueiro, S., Turon, J.L., Abrantes, F., 2014. Past circulation along the western Iberian margin: a time slice vision from the Last Glacial to the Holocene. Quat. Sci. Rev. 106, 316–329. https://doi.org/10.1016/j.quascirev.2014.09.001.
Sánchez Goñi, M.F., Desprat, S., Fletcher, W.J., Morales-Molino, C., Naughton, F., Oliveira, D., Urrego, D.H., Zorzi, C., 2018. Pollen from the deep-sea: a breakthrough in the mystery of the Ice Ages. Front. Plant Sci. 9, 38. https://doi.org/10.3389/fpls.2018.00038.
Sánchez Goñi, M.F., Harrison, S.P., 2010. Millennial-scale climate variability and vegetation changes during the Last Glacial: concepts and terminology. Quat. Sci. Rev. 29, 2823–2827. https://doi.org/10.1016/j.quascirev.2009.11.014.
Sánchez Goñi, M.F., Landais, A., Fletcher, W.J., Naughton, F., Desprat, S., Duprat, J., 2008. Contrasting impacts of Dansgaard–Oeschger events over a western European latitudinal transect modulated by orbital parameters. Quat. Sci. Rev. 27, 1136–1151. https://doi.org/10.1016/j.quascirev.2008.03.003.
Santanach, P.F., Sanz de Galdeano, C., Bousquet, J.C., 1980. Neotectónica de las regiones mediterráneas de España (Cataluña y Cordilleras Béticas). Bol. Geol. Min. 91, 417–440.
Schulz, M., Mudelsee, M., 2002. REDFIT: estimating red-noise spectra directly from unevenly spaced paleoclimatic time series. Comput. Geosci. 28, 421–426. https://doi.org/10.1016/S0098-3004(01)00044-9.
Schulz, M., Paul, A., 2002. Holocene climate variability on centennial-to-millennial time scales: 1. Climate records from the North-Atlantic realm. In: Wefer, G., Berger, W.H., Behre, K.-E., Jansen, E. (Eds.), Climate Development and History of the North Atlantic Realm. Springer, pp. 41–54.
Siani, G., Paterne, M., Michel, E., Sulpizio, R., Sbrana, A., Arnold, M., Haddad, G., 2001. Mediterranean Sea surface radiocarbon reservoir age changes since the Last Glacial Maximum. Science 294, 1917–1920. https://doi.org/10.1126/science.1063649.
Sierro, F.J., Hodell, D.A., Andersen, N., Azibeiro, L.A., Jimenez-Espejo, F.J., Bahr, A., Flores, J.A., Ausin, B., Rogerson, M., Lozano-Luz, R., Lebreiro, S.M., Hernandez-Molina, F.J., 2020. Mediterranean overflow over the last 250 kyr: freshwater forcing from the tropics to the ice sheets. Paleoceanography and Paleoclimatology 35. https://doi.org/10.1029/2020PA003931 e2020PA003931.
Sierro, F.J., Hodell, D.A., Curtis, J.H., Flores, J.A., Reguera, I., Colmenero-Hidalgo, E., Bárcena, M.A., Grimalt, J.O., Cacho, I., Frigola, J., Canals, M., 2005. Impact of iceberg melting on Mediterranean thermohaline circulation during Heinrich events. Paleoceanography 20, 1–13. https://doi.org/10.1029/2004pa001051.
Sonderegger, D.L., Wang, H., Clements, W.H., Noon, B.R., 2009. Using SiZer to detect thresholds in ecological data. Front. Ecol. Environ. 7, 190–195, 0.1890/070179.
Soon, W., Connolly, R., Connolly, M., 2015. Re-evaluating the role of solar variability on Northern Hemisphere temperature trends since the 19th century. Earth Sci. Rev. 150, 409–452. https://doi.org/10.1016/j.earscirev.2015.08.010.
Stager, J.C., Ryves, D.B., Chase, B.M., Pausata, F.S., 2011. Catastrophic drought in the Afro-Asian monsoon region during Heinrich event 1. Science 331, 1299–1302. https://doi.org/10.1126/science.1198322.
Stern, J.V., Lisiecki, L.E., 2013. North Atlantic circulation and reservoir age changes over the past 41,000 years. Geophys. Res. Lett. 40, 3693–3697. https://doi.org/10.1002/grl.50679.
Stríkis, N.M., Chiessi, C.M., Cruz, F.W., Vuille, M., Cheng, H., de Souza Barreto, E.A., Mollenhauer, G., Kasten, S., Karmann, I., Edwards, R.L., Bernal, J.P., Sales, H.d.R., 2015. Timing and structure of mega-SACZ events during Heinrich stadial 1. Geophys. Res. Lett. 42, 5477–5484A. https://doi.org/10.1002/2015GL064048.
Tinner, W., Kaltenrieder, P., 2005. Rapid responses of high-mountain vegetation to early Holocene environmental changes in the Swiss Alps. J. Ecol. 93, 936–947. https://doi.org/10.1111/j.1365-2745.2005.01023.x.
Toucanne, S., Angue Minto'o, C.M., Fontanier, C., Bassetti, M.A., Jorry, S.J., Jouet, G., 2015. Tracking rainfall in the northern Mediterranean borderlands during

sapropel deposition. Quat. Sci. Rev. 129, 178–195. https://doi.org/10.1016/j.quascirev.2015.10.016.

Turney, C., Baillie, M., Clemens, S., Brown, D., Palmer, J., Pilcher, J., Reimer, P., Leuschner, H.H., 2005. Testing solar forcing of pervasive Holocene climate cycles. J. Quat. Sci.: Published for the Quaternary Research Association 20, 511–518. https://doi.org/10.1002/jqs.927.

Van Geel, B., Raspopov, O.M., Renssen, H., van der Plicht, J., Dergachev, V.A., Meijer, H.A.J., 1999. The role of solar forcing upon climate change. Quat. Sci. Rev. 18, 331–338. https://doi.org/10.1016/S0277-3791(98)00088-2.

Voelker, A.H.L., de Abreu, L., Schönfeld, J., Erlenkeuser, H., Abrantes, F., 2009. Hydrographic conditions along the western Iberian margin during marine isotope stage 2. Geochem. Geophys. Geosyst. 10 https://doi.org/10.1029/2009GC002605.

Wagner, B., Vogel, H., Francke, A., Friedrich, T., Donders, T., Lacey, J.H., Leng, M.J., Regattieri, E., Sadori, L., Wilke, T., Zanchetta, G., Albrecht, C., Bertini, A., Combourieu-Nebout, N., Cvetkoska, A., Giaccio, B., Grazhdani, A., Hauffe, T., Holtvoeth, J., Joannin, S., Jovanovska, E., Just, J., Kouli, K., Kousis, I., Koutsodendris, A., Krastel, S., Lagos, M., Leicher, N., Levkov, Z., Lindhorst, K., Masi, A., Melles, M., Mercuri, A.M., Nomade, S., Nowaczyk, N., Panagiotopoulos, K., Peyron, O., Reed, J.M., Sagnotti, L., Sinopoli, G., Stelbrink, B., Sulpizio, R., Timmermann, A., Tofilovska, S., Torri, P., Wagner-Cremer, F., Wonik, T., Zhang, X., 2019. Mediterranean winter rainfall in phase with African monsoons during the past 1.36 million years. Nature 573, 256–260. https://doi.org/10.1038/s41586-019-1529-0.

Yu, S.-Y., Shen, J., Colman, S.M., 2007. Modeling the radiocarbon reservoir effect in lacustrine systems. Radiocarbon 49, 1241–1254. https://doi.org/10.1017/S0033822200043150.

Zhang, W., Wu, J., Wang, Y., Wang, Y., Cheng, H., Kong, X., Duan, F., 2014. A detailed East Asian monsoon history surrounding the 'Mystery Interval' derived from three Chinese speleothem records. Quat. Res. 82, 154–163. https://doi.org/10.1016/j.yqres.2014.01.010.